Semiconductor Nanowires for Energy Conversion

Allon I. Hochbaum*,[†] and Peidong Yang*

Department of Chemistry, University of California, Berkeley, California 94720 and Materials Sciences Division, Lawrence Berkeley National Laboratory, Berkeley, California 94720

Contents

1. Introduction: Role of Materials in Energy Conversion

Between 2004 and 2030 the annual global consumption of energy is estimated to rise by more than 50%.[1] Assuming current policies and practices remain in place, most of the increased energy production is expected to come from the combustion of fuels, such as oil, ethanol, natural gas, and coal. A commensurate increase in CO_2 (a prominent greenhouse gas) emissions is anticipated, much of which is due to burning coal—the fastest growing source of energy globally. Despite projected persistent increases in oil and gas prices, less than 10% of the global energy production in 2030 is predicted to come from renewable energy sources, such as hydroelectric, solar, wind, hydrothermal, and biomass. In order to moderate global reliance on exhaustible natural resources and their environmentally hazardous combustion, more scientific efforts should be directed toward reducing the cost of energy production from renewable sources.

There exist many potential renewable energy technologies in the form of solid-state devices, such as, for example, solar cells, which convert solar energy in the form of light to the more practical form of electricity. In addition, a large collection of condensed matter phenomena involve the conversion of energy from one form to another, and some proceed with efficiency near unity. Consequently, the study of energy conversion in materials is a field full of opportunities for practical and socially significant applications. Within the last couple of decades there has been increasing interest

* To whom correspondence should be addressed. E-mail: hochbaum@seas.harvard.edu (A.H.), p_yang@berkeley.edu (P.Y.).
[†] Current address: School of Engineering and Applied Sciences and Department of Chemistry and Chemical Biology, Harvard University, Cambridge, MA 02138.

in materials with nanometer-scale dimensions. Semiconductor nanowires, a subset of these materials, have received exceptional attention for their unique properties and complex structures. Many nanowire-based materials are promising candidates for energy conversion devices.

Since electricity is ubiquitously used to power machines and instruments which do work for humans, the practical end product of many energy conversion processes is electrical energy. Even in devices which produce other forms of energy, such as chemical fuel, the conversion process often requires, at least as an intermediate energy state, an electrical potential. For nanowire materials, a fundamental understanding of transport in quasi-one-dimensional structures will be crucial to the development of new energy conversion technologies. Moreover, as global power consumption increases, there will be an increasing need for new energy storage schemes. Pushing electrons across power grids may not be the ideal solution for many alternative energy technologies. Rather, electrical energy storage in batteries and chemical fuels seems to be a fruitful research direction. To this end, a fundamental understanding of the electrochemical properties and electron transfer characteristics of nanostructured electrodes and catalysts will be essential. The following sections will review ways in which semiconductor nanowires can enable advanced solid-state energy conversion and storage devices. The discussion of nanowire-based devices will focus on photovoltaic, thermoelectric, and chemical energy storage materials, namely, the conversion of light energy, heat energy, and the energy stored in chemical bonds to electrical potentials and vice versa.

2. Why Are Semiconductor Nanowires Special?

The term 'nanowire' is generally used to describe a large aspect ratio rod 1−100 nm in diameter (Figure 1). Both descriptors are pertinent to the physical and technological significance of nanowires. First, the diameter puts the radial dimension of these structures at or below the characteristic length scale of various interesting and fundamental solid-state phenomena: the exciton Bohr radius, wavelength of light, phonon mean free path, critical size of magnetic domains, exciton diffusion length, and others.[2,3] As a result, many physical properties of semiconductors are significantly altered within the confines of the nanowire surfaces. In addition, their large surface-to-volume ratio allows for distinct structural and chemical behavior as well as greater chemical reactivity. This two-dimensional confinement endows nanowires with unique properties which stray from those of their corresponding bulk material. Second, the large aspect ratio of nanowires intimates their technological application. The one unconstrained dimension can direct the

Allon Hochbaum received his S.B. degree in Materials Science and Engineering from the Massachusetts Institute of Technology in 2003. He joined Professor Peidong Yang's lab and received his Ph.D. degree from the Department of Chemistry at U.C. Berkeley in 2008, partly funded by an NSF IGERT fellowship in Nanoscience and Nanotechnology. He is currently a postdoctoral research fellow at Harvard University, investigating biological and materials interfaces. His research interests include the design and synthesis of nanometer-scale materials with unique properties for energy conversion and biological applications.

Peidong Yang received his B.S. degree in Chemistry from the University of Science and Technology of China in 1993 and Ph.D. degree in Chemistry from Harvard University in 1997. He did postdoctoral research at the University of California, Santa Barbara, before joining the faculty in the Department of Chemistry at the University of California, Berkeley, in 1999. He is currently Professor in the Department of Chemistry, Materials Science and Engineering, and a senior faculty scientist at the Lawrence Berkeley National Laboratory. He is the deputy director for the Center of Integrated Nanomechanical Systems. He is an associate editor for the *Journal of the American Chemical Society* and also serves on the Editorial Advisory Board for a number of journals including *Accounts in Chemical Research* and *Nano Letters*. He was the first chairperson for the newly established Nanoscience subdivision within the American Chemical Society. He is the recipient of the Alfred P. Sloan research fellowship, Arnold and Mabel Beckman Young Investigator Award, National Science Foundation Young Investigator Award, MRS Young Investigator Award, Julius Springer Prize for Applied Physics, ACS Pure Chemistry Award, and Alan T. Waterman Award. His main research interest is in the area of one-dimensional semiconductor nanostructures and their applications in nanophotonics, nanoelectronics, energy conversion, and nanofluidics.

conduction of quantum particles such as electrons, phonons, and photons. This control over various forms of energy transport recommends nanowires as ideal materials from which to manufacture advanced solid-state devices. Moreover, nanowire lengths are normally sufficient to interface with top-down fabrication processes, such as photolithography. As a result, nanowires provide a convenient platform through which researchers may study confined transport phenomena.
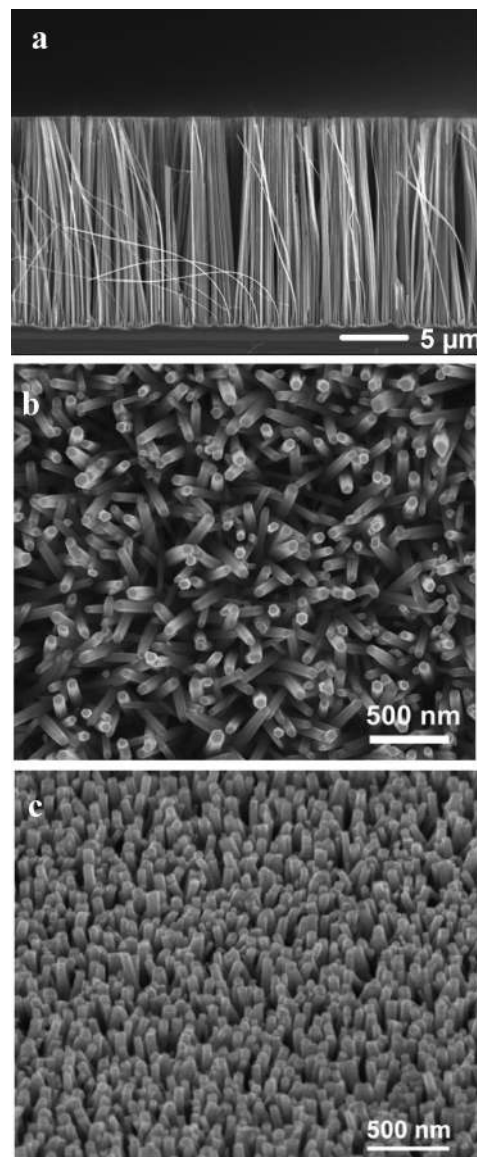

Figure 1. Scanning electron microscopy images of Si, ZnO, and InGaN nanowires, important semiconductor materials for energy conversion and storage.

3. Electrical and Thermal Transport in Nanowires

For the past decade, exquisite synthetic control has enabled researchers to specifically tailor nanowire structures and observe a wide range of electron transport phenomena. By fine tuning high-quality heterostructures and interfaces within nanowires, researchers have been able to track single-electron transport. With small nanowire diameters, the volume occupied by conduction electrons is significantly condensed. When the longitudinal dimension is also constrained, in this case by the electronic band offset between axial heterojunctions, these electrons interact more strongly and repel each other. In such cases, discrete amounts of energy are required to push electrons into these confined volumes and individual electrons can be manipulated by applied voltages.[4] Electron transport phenomena such as Coulomb blockades[5,6] and resonant tunneling[7] have been observed in such systems. These properties are useful for fabricating advanced solid-state devices such as resonant tunneling diodes[7] and single-electron transistors.[8] Additionally, coaxial heterostructures can be fabricated controllably to produce a one-dimensional hole gas, which is useful for high-performance field-effect
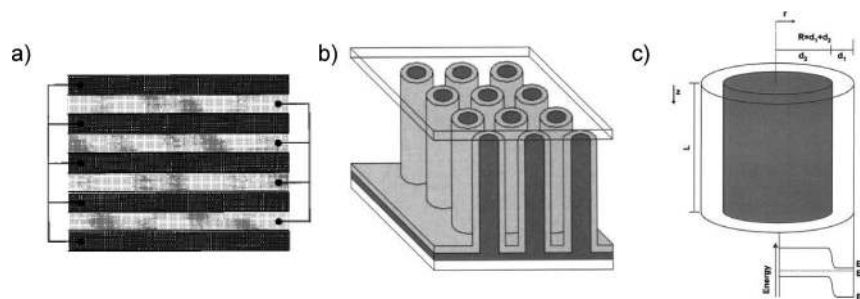
Figure 2. Heterojunction morphologies for improved charge collection. (a) Multilayer heterojunctions require multiple deposition steps and postgrowth processing to contact individual layers. (b) Vertically aligned radial heterostructures require minimal processing steps and successfully decouple the absorption and minority charge carrier diffusion lengths. (c) The diameter of the p- and n-type core and shell can be optimized depending on the trap density in the layers. (Reprinted with permission from ref 15. Copyright 1995 Wiley. Reprinted with permission from ref 17. Copyright 2005 AIP.)

transistors.[9] Nanowires have also been shown to support correlated electron transport, such as superconductivity.[10] Synthetic techniques have been developed to the point where electronic confinement and unique properties are readily achieved, and ongoing research is in finding new ways to use and integrate these nanowires into functional devices.

Interesting size-dependent behavior has also been observed for thermal transport in nanowires. Li and co-workers[11,12] discovered that the thermal conductivity of vapor−liquid−solid (VLS) grown Si nanowires is strongly diameter dependent. They found that the thermal conductivity of small diameter nanowires is up to 10-fold lower than the bulk value. Furthermore, the temperature dependence of the thermal conductivity at low temperature is highly anomalous for thin wires. Whereas the thermal conductivity is expected to scale as $\sim T^3$, following the low-temperature heat capacity, it scales as $\sim T^2$ or even linearly with temperature for the smallest diameter nanowires. Though this phonon transport is not as well understood as nanoscale electronic phenomena, these results suggest that heat conduction in confined systems is a relatively unexplored and intriguing field of study. It is these unique charge and thermal transport phenomena that make semiconductor nanowires promising as building blocks for many of the energy conversion and storage devices reviewed in this manuscript. Not all energy conversion schemes are put to use, many as a result of prohibitive costs. Consequently, the goal of much of the following work is twofold: (1) to study fundamental energy conversion processes in high-quality, well-characterized nanowire systems and (2) to exploit the size dependence of nanowire transport properties to fashion efficient devices using inexpensive and scalable materials and syntheses.

4. Nanowire Photovoltaic Devices

4.1. Conventional Solar Cells

Although most commercial solar cells are fabricated from silicon, it has a relatively low absorption coefficient throughout much of the visible and near-infrared parts of the electromagnetic spectrum.[13,14] Because the vast majority of the light from the sun is in this range, silicon-based solar cells must be thick in order to collect most of the incident photons. For example, a silicon cell must be several micrometers to millimeters thick to absorb 90% of the incident light at wavelengths from 700 to 1100 nm, respectively, which comprise about one-half of the solar energy available above the band gap of silicon.[13,15] Conventional solar cells are constructed from planar junctions of p- and n-type semiconductors, where the electrostatic potential at the interface provides the driving force for charge separation. The collection efficiency of charge carriers generated at a given distance from the junction, though, depends on the minority carrier diffusion length in the n- and p-type quasi-neutral regions. The minority carrier diffusion length is limited by various recombination mechanisms within the silicon lattice and their associated relaxation times. To minimize carrier recombination and thus optimize collection efficiency, cells must be constructed of high-purity single-crystalline silicon with a large minority carrier diffusion length. Though highly efficient cells have been fabricated in the laboratory, practical application of such devices is limited due to the cost of producing and refining such pure material and the associated device fabrication.

A proposed solution to this problem relies on decoupling the long extinction distance of silicon and the proximity of generated charge carriers to the p−n junction. Devices that absorb photons and collect charges along orthogonal directions meet this condition. Parallel multijunction cells, for example, address this issue by connecting thin, alternating n- and p-type vertically stacked layers in parallel with charges extracted laterally.[16] Though such devices have theoretical charge collection efficiencies near unity and are highly defect tolerant, the fabrication process requires multiple thin-film deposition steps that may preclude their widespread use. Such a scheme can also be realized by fabricating p−n junctions that lie normal to the substrate surface, such as an array of silicon posts composed of core and shell regions of opposite carrier polarity,[17] as shown in Figure 2. Charges generated in this structure could be extracted from both quasi-neutral regions by contacting separately the substrate, connected to the core, and the top surface of the posts, connected to the shell. Although synthetic methods such as VLS-CVD growth could be used to fabricate such arrays, the required dimensions for these structures are not necessarily nanometer scale.[18] The optimal post diameter is about twice the minority carrier diffusion length, which is hundreds of nanometers to several micrometers even at high carrier densities ($\sim 10^{18}$ cm^{-3}).[17,19] Even bottom-up-synthesized silicon nanowires, which may contain high concentrations of metal impurity trap sites, exhibit minority carrier diffusion lengths up to several micrometers that appear to be surface-recombination limited.[19,20] At this size scale, these post arrays should be attainable with conventional top-down photolithographic methods.

Truly nanoscale wires offer performance enhancements when the minority carrier diffusion length drops significantly
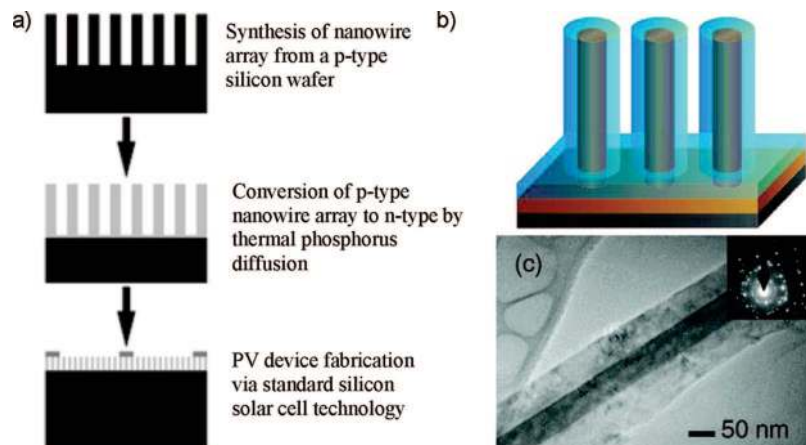
Figure 3. Nanowire array solar cells. (a) Schematic of a subsurface p−n junction device fabrication process. (b) Schematic of a radial heterostructure nanowire array, and TEM image of one of the synthesized nanowires showing the n-type crystalline core and p-type polycrystalline shell. (Reprinted with permission from ref 29. Copyright 2005 Wiley. Reprinted with permission from ref 38. Copyright 2008 American Chemical Society.)

as is the case with highly defective silicon. For many applications the critical parameter of power generation is cost per Watt. Even relatively inefficient solar cells, therefore, are practical as long as their fabrication costs are low enough. The cost of silicon and substrate processing comprises 10−50% of the total cost of a solar cell,[14,21,22] and much of the cost is due to the purification process, as metallurgical grade silicon (99−99.99% purity, or about $10^{19}-10^{21}$ impurities per cm³) is 50 times less expensive than higher grade silicon.[23] Consequently, the price per Watt of power from conventional solar cells could drop significantly if these devices tolerated higher defect concentrations.[24] The power conversion efficiency of a solar cell is given as $\eta = (FF|J_{SC}|V_{OC})/P_{in}$, where FF is the fill factor, J_{SC} is the current density at short circuit ($V = 0$), V_{OC} is the photovoltage at open circuit ($I = 0$), and P_{in} is the incident light power density. The main cause of efficiency losses from lattice defects in silicon solar cells is an increase in the recombination current resulting from minority carrier recombination at trap sites. Recombination currents can account for a 25% or more decrease in overall cell efficiency, depending on the energy of the impurity acceptor or donor states, due to lower V_{OC} and FF.[25,26] This recombination current varies as $I_{rec} \propto (L_n L_p)^{-1}$, where $L_{n/p}$ is the minority carrier diffusion length for n- or p-type carriers and $L_{n/p} \propto N_t^{-1/2}$, where N_t is the carrier trap density.[26,27] Photovoltaic devices made from nanostructured dirty silicon would benefit from shorter minority carrier conduction lengths that might mitigate this problem.

Several studies of silicon nanowire-based solar cells primarily explore the advantages of greater light absorption within the nanowire array. The vertical array geometry scatters light efficiently, especially at short wavelengths, and, depending on the nanowire dimensions, can absorb more light than a comparably thick solid crystalline film.[28] This result has been born out in several studies where the p−n junction lies below the surface of the wafer upon which the array stands.[29−31] Since nanowires do not span the junction in these devices, the cells behave like conventional single-crystalline p−n junction cells, only with greater absorption of incident light. These cells, schematically shown in Figure 3a, do not reach the efficiencies of conventional cells for a couple reasons. First, the junctions made in the lab by diffusion doping are generally of poor quality, so the V_{OC} suffers significantly.[29,31] Second, charge extraction occurs

through the nanowires, decreasing J_{SC} due to the larger series resistance of the nanowires and their contacts. The latter effect is especially pronounced in the VLS-grown nanowires[30,32] because they cover very little of the substrate surface, thus reducing the conduction cross-section. Consequently, their efficiencies are 0.1% or less. Mg-doped GaN nanowires grown on silicon substrates have analogous antireflection properties and power conversion efficiencies of nearly 3%.[33] These cells also possess larger internal fields, improving V_{OC} to 0.95 V. This work is also promising for fabricating photovoltaic devices with lattice-mismatched materials since nanowires can withstand more strain than corresponding thin films.[34−36]

Silicon nanowire radial heterostructures, on the other hand, are the optimal design for efficient charge collection. These structures have been realized with VLS-grown[32,37] and electrolessly etched silicon nanowire arrays.[38] Both methods first synthesize the nanowires and then deposit conformal polycrystalline thin films of intrinsic or complementary polarity silicon. Garnett and co-workers fabricated radial p−n junctions, shown in Figure 3b and c, on nanowire arrays synthesized by a scalable, aqueous solution etching synthesis[39] which exhibit cell efficiencies of about 0.5%. The low efficiency is due partly to interfacial recombination losses (decreasing V_{OC} and FF), as evidenced by a significant dark current, and partly to a large series resistance in the polycrystalline shell (decreasing J_{SC}).[38] Tian and co-workers synthesized similar nanowires with p−n and p−i−n radial heterostructures by the VLS mechanism and subsequent thin film deposition and characterized the photovoltaic response of individual nanowires (Figure 4). Though V_{OC} and J_{SC} were not reported for the p−n device, it is clear from the ideality factor and breakdown voltage that the p−i−n heterostructure contains a more robust junction. The V_{OC} of this device is similar to the radial p−n nanowire arrays of Garnett et al., but J_{SC} is four to five times greater, possibly a result of significantly lower polycrystalline shell resistivity. The device efficiency was calculated to be between 2.3% and 3.4%. Additionally, Tian and co-workers demonstrated a single-nanowire photovoltaic device by selective chemical etching and contacting the p- and n-type regions separately. Moreover, this device was able to power a logic circuit and a nanowire pH sensor on a self-contained circuit.[37]
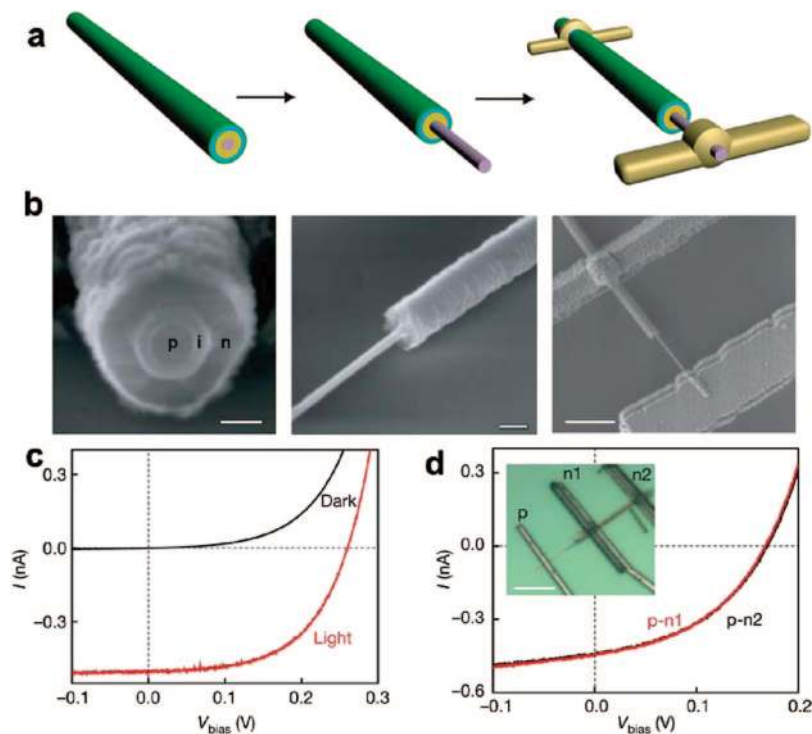
Figure 4. (a) Schematics of single nanowire PV device fabrication. (Left) Pink, yellow, cyan, and green layers correspond to the p-core, i-shell, n-shell, and PECVD-coated SiO_2, respectively. (Middle) Selective etching to expose the p-core. (Right) Metal contacts deposited on the p-core and n-shell. (b) SEM images corresponding to schematics in a. Scale bars are 100 nm (left), 200 nm (middle), and 1.5 μm (right). (c) Dark and light $I-V$ curves. (d) Light $I-V$ curves for two different n-shell contact locations. (Inset) Optical microscopy image of the device. Scale bar, 5 μm. (Reprinted with permission from ref 37. Copyright 2007 Nature.)

4.2. Excitonic Solar Cells

Another type of photovoltaic device, known as an excitonic cell,[40,41] in which small molecules, polymers, or quantum dots are used as light absorbing materials, could also benefit from incorporation of nanowire components. Electronic excitations, by incident light, in these cells produce bound electron−hole pairs called excitons. For comparison, excitons in silicon have a binding energy of roughly 20 meV, whereas thermal energy at room temperature (kT) is approximately 25 meV. Consequently, illumination of silicon generates free carriers in the bulk, which segregate to the electrodes due to the built-in potential of the p−n junction. In contrast, the weak intermolecular interactions and low dielectric constants of organic dyes, small molecules, and polymers lead to greater localization of photoexcited states.[42] With exciton binding energies greatly exceeding kT, illumination of excitonic solar cells generates tightly bound electron−hole pairs. In order to separate charge, the exciton must diffuse to the junction without recombining. Exciton dissociation occurs as long as the band offset energy at the junction is greater than the exciton binding energy in the material from which it was generated. The exciton splitting in these devices is further limited by the kinetics of charge injection through the junction. As a result, the V_{OC}, and partly J_{SC}, depend on the relative rates of electron and hole transfer across the interface.[41]

Using an orthogonalized geometry, like in conventional cells, efficiency improvements may be realized in excitonic solar cells by making the junction normal to the substrate.[43] The critical dimension for these photovoltaic devices is the exciton diffusion length, which is typically much shorter, roughly 10 nm or less in polymers and up to a micrometer in high-quality small molecule films, than the minority carrier diffusion length in silicon.[41,44] This device structure maxi-

mizes the volume of the absorber material and/or interfacial area which contribute to charge generation while providing high-mobility channels through which these charges can be extracted.[43] Excitonic cells are promising due to their use of inexpensive organic materials such as dyes and polymers, and those that employ inorganic components generally use scalable solution syntheses. Features of the size, spacing, and aspect ratio required for efficient excitonic devices are currently accessible only through bottom-up synthetic approaches.

4.2.1. Polymer−Inorganic Hybrid Cells

Recent research on hybrid organic−inorganic solar cells has generated promising devices for inexpensive, large-scale solar energy conversion, in contrast to the high materials and production costs of the solid-state inorganic devices described above. While many semiconducting small molecules have superior electronic and optical properties, they are typically deposited by high-vacuum evaporation. Most relevant polymers, on the other hand, are soluble in organic solvents and can be cast onto any substrate in a variety of ways, including manufacturing-friendly roll-to-roll processes. In addition, these polymers generally have high absorption coefficients above 10^5 cm^{-1}.[42] Consequently, polymer-based solar cells can be much thinner, tens to hundreds of nanometers, than many of their inorganic counterparts. The short extinction length is fortunate because the exciton diffusion length in polymers is typically less than 10 nm[44] and the hole mobility in most polymeric devices is $10^{-1}-10^{-7}$ cm^2 V^{-1} s^{-1},[45] as compared to about 500 cm^2 V^{-1} s^{-1} in silicon. As a result, an optimal solar cell thickness arises from a balance of several parameters: the cell should be thick enough to maximize absorbance but thin enough maximize the exciton dissociation interface area and mini-
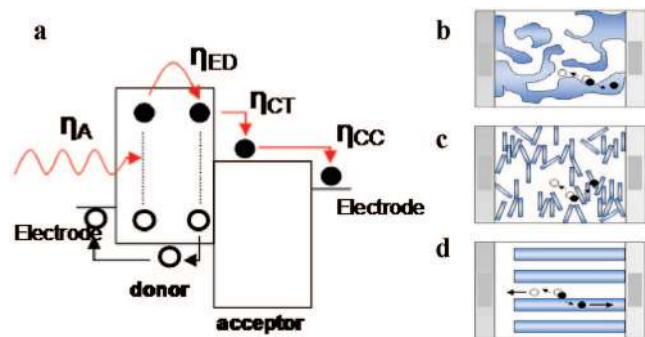
Figure 5. (a) Schematic illustration of typical band gap arrangement in a bulk heterojunction solar cell. (b−d) Diagrams of three types of donor−acceptor heterojunction photovoltaic cells: (b) polymer blend cell, (c) nanorod−polymer cell, and (d) ordered nanowire−polymer cell. In these drawings, electrons (filled circles) and holes (open circles) liberated from excitons (paired circles) split at the donor−acceptor interface must travel a convoluted path to reach the electrodes in either b or c, while the direct channels present in d result in short diffusion times and efficient charge collection.

mize the series resistance of the cell. Devices similar to conventional parallel multijunction cells have been produced to decouple these design parameters from film thickness.[46,47] The poor exciton and charge transport in polymer photovoltaic devices, though, suggests nanowire array anodes are the ideal structures to maximize their efficiency.[43,45]

Several groups have demonstrated prototype cells that utilize nanostructured blends of materials such as polymers, fullerene derivatives, and/or nanorods which avoid most of the costly fabrication associated with conventional Si and CdTe photovoltaics. Most hybrid devices comprise an interpenetrated network of electron donor and acceptor materials, called a bulk heterojunction, where the band offset at the extended interface induces dissociation of photogenerated excitons, as shown schematically in Figure 5a. The bulk heterojunctions used in organic,[48] nanorod−polymer,[49] and fullerene−polymer[50,51] photovoltaic cells are formed via phase separation during spin coating of mixtures of complementary donor and acceptor materials. These cells have much higher efficiencies than those based on single-component polymer films, but they are limited by inefficient charge transport due to the discontinuous percolation pathways, as shown schematically in Figure 5b and c. Ordered inorganic nanowire arrays can potentially address this issue, employing device morphologies like the one depicted in Figure 5d.

The external quantum efficiency of an excitonic solar cell is given by $\eta_{EQE} = \eta_A\eta_{ED}\eta_{CC}$, where η_A is the photon absorption efficiency, η_{ED} is the efficiency of exciton dissociation, and η_{CC} is the fraction of carriers collected by the electrodes of the device (Figure 5a). In a planar junction cell of total thickness L and average optical absorption length L_A, the absorption efficiency is approximately $\eta_A = 1 - \exp(-L/L_A) > 50\%$, while the charge collection efficiency is nearly 100%. However, since the exciton diffusion length, L_{ED}, is typically an order of magnitude smaller than L_A, the majority of photogenerated excitons are lost before reaching a donor−acceptor interface, resulting in a low η_{ED} and a low power conversion efficiency. Bulk heterojunctions in organic and inorganic−organic hybrid cells alleviate the limitation on film thickness of planar cells.[51] In a bulk heterojunction, the majority of excitons are generated within a distance L_{ED} of a dissociation site. Strong quenching of the photoluminescence in these films indicates that η_{ED} approaches unity,[50]

and conversion efficiencies as high as 5% have been reported.[52,53] Instead of a poor exciton dissociation rate, these films have poor charge transport characteristics, causing space−charge-limited currents and low efficiencies.[54,55] High-density nanowire arrays can improve charge conduction, especially in thick films for maximal absorption, while providing enough surface area to maintain a high η_{ED}.

Bulk heterojunction cells with inorganic electron transporting materials have been fabricated from TiO$_2$[56,57] and ZnO[58] nanoparticle networks and ordered TiO$_2$ mesoporous films.[45] In these devices the inorganic component acts as the electron conduction medium. In polymer cells using narrower band gap materials such as CdSe,[49,59,60] PbS,[61] and PbSe,[62] the nanoparticle phase is both a complementary absorber and an electron transporter. By expanding the spectral range of absorption of the cell, these devices achieved nearly double the efficiency, up to 2.6%,[63] of those with wide band gap inorganic components. Charge separation and tunneling transport in polymer−inorganic hybrid devices[45,55,57,64] is similar to most excitonic and dye-sensitized solar cells (DSSCs), only nanoparticles in these cells do not have the advantage of charge screening and depletion that make DSSCs so efficient. Exciton dissociation in these devices is about 1000 times slower (1 ns)[65] than in the fastest polymer bulk heterojunctions[66−68] and is limited by potential barriers at the interface[60,69] and the nonideal density-of-states overlap between the polymer and inorganic phase. Electron transport and recombination rates, on the other hand, are extremely sensitive to the nanoparticle morphology, with directional and elongated nanorod structures significantly improving cell efficiencies.[49,54,65,70] For a review of other semiconductor nanocrystal- and carbon nanotube-polymer hybrid devices, see ref 71.

The field of inorganic nanowire−polymer hybrid solar cells is not as advanced as that of nanowire DSSCs, possibly due to the low overall efficiencies. Whereas DSSCs debuted at 7% power conversion efficiency in 1991,[72] even the best polymer bulk heterojunction cells barely reach 5%.[52,53] Polymer hybrid photovoltaics, however, promise to be one of the least expensive and easily manufactured classes of nanowire solar cells and therefore merit more attention. The first example of such devices was composed of electrodeposited CdTe in an anodized alumina template with poly(3-octylthiophene) as the hole-conducting polymer.[73] Though these polycrystalline nanowires likely did not have as low a series resistance as single-crystalline nanowires would have, they benefited from additional absorption in the CdTe and exhibited a respectable efficiency of about 1%. Cells have since been fabricated from polycrystalline transparent conductors such as TiO$_2$[74,75] and ZnO[76] using poly(3-hexylthiophene) (P3HT) as the absorber and show efficiencies of about 0.5%, a 2- to 4-fold improvement over planar control devices.

Single-crystalline nanowire (or nanorod, since due to the thin devices the aspect ratio of the inorganic phase is generally 10 or less) arrays of ZnO[77−79] and InP[80] have been recently used in polymer hybrid cells to speed electron conduction to the anode. The ZnO nanorods can be synthesized by a hydrothermal method on conducting glass or plastic substrates, yielding arrays of 20 nm diameter × 250 nm length rods with a packing density of roughly 4×10^{10} cm^{-2}.[81,82] The surface area of nanorod substrate is about 10 times that of a flat surface of the same projected area, and the internanowire spacing is 10−20 nm on average, which
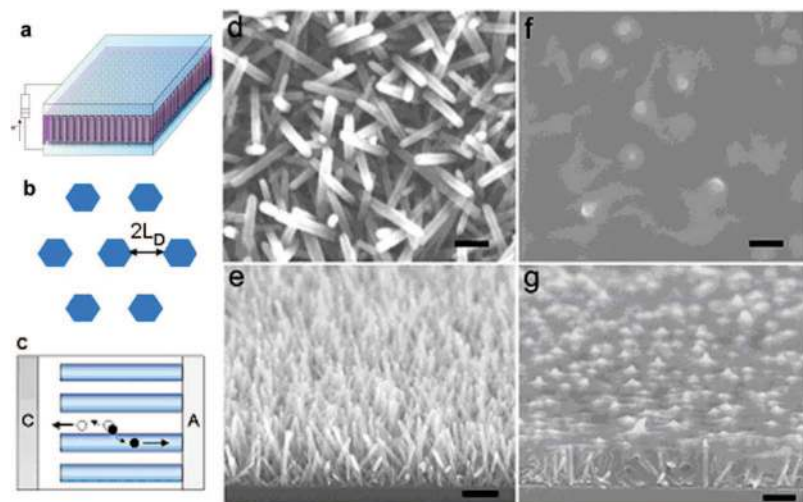
Figure 6. Diagrams of nanowire-based donor–acceptor heterojunction photovoltaic cells and SEM images of the organic–inorganic composite. (a–c) Diagrams for ordered nanowire–polymer cell. (d–g) SEM images. (d) Plan view image of a bare ZnO nanowire array. (e) Cross-section of the same array on a silicon wafer, tilted 15°. (f) Plan view after melt casting the P3HT film. (g) Cross-section of the nanowire–polymer composite. Scale bars in the top two images represent 100 nm and 200 nm in the bottom two images.
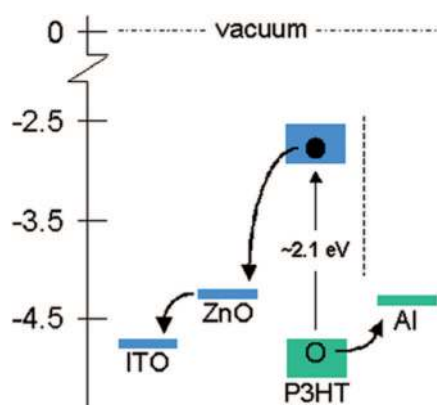

Figure 7. Simplified band diagram for the ZnO nanowire–polymer solar cell. Excitons are generated in the P3HT and split at the nanowire surface.

is comparable to the typical exciton diffusion length of the typical polymer absorber. The nanowire–polymer bulk heterojunctions are formed by spin coating regioregular P3HT (RR-P3HT) onto clean ZnO wire arrays. RR-P3HT is a conjugated, photostable conducting polymer with a large, for polymers, hole field-effect mobility of 0.2 cm^2 V^{-1} s^{-1} [83] and a relatively narrow band gap of 2.14 eV.[84] Annealing cast films to the melting point of P3HT followed by slow cooling allowed the polymer to fully penetrate the nanorod array with good wetting of the ZnO surface (Figure 6). The polymer volume should sufficiently cover the nanorods but not form too thick of a layer so as to impede charge conduction to the electrode.

The energetic and geometric parameters affecting the exciton dissociation efficiency, η_{ED}, are vital to the performance of hybrid cells. Exciton splitting at the ZnO/P3HT interface is both thermodynamically and kinetically favored.[85] A simplified band alignment picture is given in Figure 7. η_{ED} of these films was measured by comparing their quenched photoluminescence (PL), due to charge separation instead of radiative recombination, relative to the emission of neat P3HT films. Normalized PL spectra of filled arrays before and after the melting treatment indicate that nearly 30% of the excitons that decay radiatively in the planar film are split at the donor–acceptor interface in the nanowire

composite. X-ray diffraction patterns show that the polymer is crystalline, and absorption measurements show no evidence of the blue shift characteristic of poor RR-P3HT crystallization, suggesting that the polymer likely retains a high hole mobility.[79]

Greene and co-workers found that adding a ∼5 nm polycrystalline TiO$_2$ shell improved the efficiency of their devices 5-fold, primarily due to increases in V_{OC} and FF.[79] This effect was ascribed to poor interface charge separation between P3HT and ZnO. Plank and co-workers observed similar results and came to the same conclusion with ZnO–MgO core–shell structures in cells incorporating an absorbing dye at the interface.[86] Neither of these materials, however, produced devices with efficiencies above 0.4%, mostly due to the small volume of polymer between neighboring nanowires. Polymer confinement can also lead to conformational changes that are detrimental to exciton diffusion and hole transport.[87] The independence of J_{SC} on polymer thickness in the cells of Greene et al. supports this result and suggests that inefficient exciton dissociation, rather than charge transport, is responsible for the poor device performance.

The highest efficiencies for nanowire–polymer hybrid cells have been measured in devices using bulk heterjunction polymer films. Using ZnO nanowires predominantly as electron conductors, rather than an interface for charge separation, these cells operated at between 2% and 4% efficiency.[88–90] With films of P3HT:PCBM, Takanezawa and co-workers demonstrated higher efficiencies corresponding to longer nanowires, suggesting that the ZnO behaves as a better charge conductor than the PCBM. In this case, the majority of the exciton dissociation occurred at the P3HT–PCBM interface, which is known to separate charge efficiently, and electrons were subsequently shuttled from the PCBM to the nanowires.[89] The inorganic phase may also be responsible for exciting extra charge carriers, which can contribute to the device J_{SC}. This strategy seems to be a promising way to decouple the poor charge separation properties of the nanowire–polymer interface from the superior charge conduction of the nanowires and may be the ideal route to efficient and inexpensive inorganic–polymer hybrid solar cells.

4.2.2. Dye-Sensitized Solar Cells

Another example of an excitonic cell is the dye-sensitized solar cell (DSSC),[40,72,91] in which light-absorbing dye molecules decorate high surface area films of an inorganic, electron-conducting phase. The DSSC is currently the most efficient[92,93] and stable[94] excitonic cell. Light absorption in these cells is limited to the dye monolayer, which subsequently oxidizes a liquid electrolyte and transfers electrons to the inorganic phase. DSSC anodes are typically constructed of nanoparticle films several micrometers thick or more. These films are typically composed of TiO_2,[95] but also SnO_2[96] or ZnO,[97] nanoparticles to achieve high surface area supports for the dye monolayer. The high dye concentration yields optically thick anodes with large light absorption in the 400−800 nm region, where a large portion of solar energy is incident. Upon charge separation, electrons conduct by diffusive tunneling, "hopping", transport through the percolation network of nanoparticles.[40,98] The films must be thick to maximize the path length of incident light and hence the absorption by the dye, which is particularly inefficient in the red and near IR. Inefficient electron transport, however, prevents cells from being thicker due to low electron diffusion constants and recombination losses.[99−104]

Compared to single-crystalline ZnO and TiO_2, nanoparticle films of these materials exhibit significantly slower charge transport. Time-resolved photocurrent and photovoltage measurements[99,105] and modeling efforts[106,107] indicate that electron transport in wet, illuminated nanoparticle networks occurs by a trap-limited diffusion process. Drift transport, i.e., in response to an electric field, is prevented in DSSCs by ions in the electrolyte that screen macroscopic electric fields.[108] The electron diffusion coefficients are several orders of magnitude lower in nanoparticle devices ($D < 10^{-4}$ cm^2 s^{-1})[109−113] as compared to TiO_2[114] and ZnO[115] single crystals. Remarkably, the charge collection efficiency of these films is high due to the slow kinetics of the back reaction of injected electrons with the electrolyte, typically I_3^- reduction at the anode surface.[108] The electron diffusion lengths in these devices are accordingly long, up to several tens of micrometers at low illumination intensities.[94,116,117] However, current research efforts on DSSC improvements focus on the development of new dyes[118−121] and electrolytes,[122,123] thus changing the kinetics of the forward and reverse redox reactions.[124] In these and other cases where surface recombination becomes significant, such as in polymer−inorganic hybrid cells, the low electron diffusion coefficient values become significantly more detrimental to device performance.

Single-crystalline ZnO nanowires, on the other hand, are excellent conductors. Electrical measurements of dry arrays on conductive glass give linear I−V traces that indicate an ohmic contact between the nanowires and the substrate. The transport properties of individual nanowires were measured using field-effect devices fabricated by electron beam lithography, as shown in Figure 8. The resistivity values of as-grown ZnO nanowires ranged from 0.3 to 2.0 Ω cm, falling on the conductive end of the spectrum for nominally undoped ZnO.[125] The carrier concentration was about 5 × 10^{18} cm^{-3}, and a field-effect mobility of 1−5 cm^2 V^{-1} s^{-1} was calculated for typical devices from the transconductance plots. Using the Einstein relation, $D = kT\mu/e$, where D is the diffusion constant, kT is the thermal energy, μ is the mobility, and e is the elementary charge, the electron diffusion coefficient for individual dry nanowires was calculated to be 0.05−0.5 cm^2 s^{-1}. These diffusion coef-
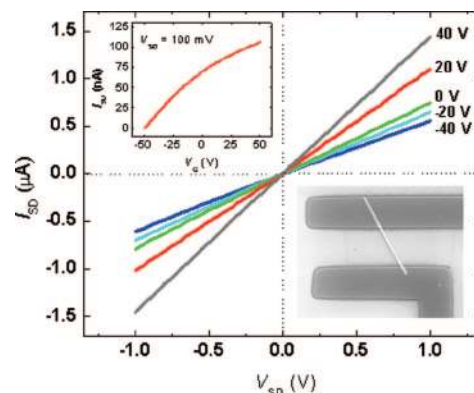

Figure 8. Single ZnO nanowire electrical characteristics. I−V curves at various gate biases for a nanowire with a diameter of 75 nm, showing n-type behavior and a zero-gate resistivity of 0.65 Ω cm. (Right inset) SEM image of a nanowire device. (Left inset) Transfer plot (I_{SD} vs V_G) of a nanowire FET, taken at $V_{SD} = 100$ mV. The ON−OFF ratio in this case is 10^5 at ±50 V. (Reprinted with permission from ref 127. Copyright 2005 Nature.)

ficients are several orders of magnitude greater than those found in nanoparticle films and indicate that ZnO nanowires are superior electron conductors.

Structurally, nanowire array-based DSSCs are like nanoparticle DSSCs with the particles assembled into columns and without grain boundaries, thus forming direct conduction channels, a highway for electrons. However, there are fundamental differences in the physics which govern the nanowire device behavior. First, unlike the mesoporous nanoparticle films, the mean nanowire diameter is thick enough to support a depletion layer near the surface. This potential barrier can provide an energetic driving force for exciton dissociation at the interface between the ZnO and the dye, making charge injection more efficient. Also, band bending sweeps electrons away from the surface, potentially reducing the rate of recombination. Second, because electrons in the nanowires are not isotropically screened by counterions in the electrolyte, these DSSCs can sustain an internal electric field along the axis of the nanowires. As a result, electrons injected into the nanowires drift toward the substrate electrode, down the chemical potential gradient. Furthermore, electron mobility in the nanowire is larger than that in the particle films due to their directional and uninterrupted conduction channel, as opposed to the tortuous percolation network and grain boundaries of the nanoparticle films. This directed transport is expected to increase the electron diffusion constant, thus improving the efficiency of charge collection and enabling the production of optically thick cells which absorb more incident light. The schematic comparison of such devices is shown in Figure 9.

Nanowire-based DSSCs were first realized with vertically oriented, single-crystalline ZnO nanowire arrays,[81,82,126−128] with efficiencies from 0.5%[128] to 1.5%.[127] Solar cells were fabricated from nanowire arrays of various lengths and tested under AM 1.5 illumination. Longer nanowires performed better, with record cells having $J_{SC} = 6.0$ mA cm^{-2}, $V_{OC} = 0.68$, $FF = 0.45$, and a power conversion efficiency of 1.5%. The external quantum efficiency of these cells peaks at 45% near the absorption maximum of the dye.[127] The open-circuit voltage is about 0.1 V better in the nanowire cell, likely a result of lower recombination losses. The low short-circuit current and quantum efficiency, as compared with the best TiO_2 nanoparticle devices, are due to the smaller total surface area of the nanowire array. The nanoparticles, having a
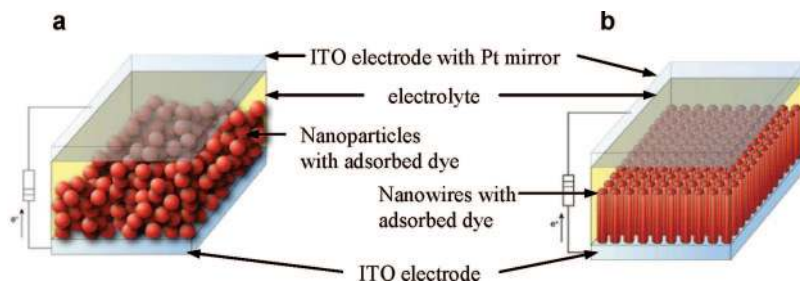
Figure 9. Schematic representations of a DSSC. (a) Traditional cell (nanoparticle film electrode). (b) Nanowire DSSCs.
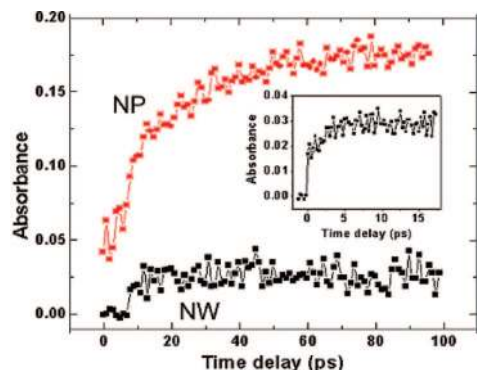

Figure 10. Transient mid-IR absorption traces of dye-sensitized ZnO nanowire (NW) and nanoparticle (NP) films pumped at 400 nm. The large difference in injection amplitudes is due to the much larger dye loading of the particle film. Injection in wires is complete after ~5 ps but continues out to ~100 ps in the particle case. A high-resolution trace (inset) shows the ultrafast step (<250 fs) and ~3 ps rise time for a nanowire sample. (Reprinted with permission from ref 127. Copyright 2005 Nature.)
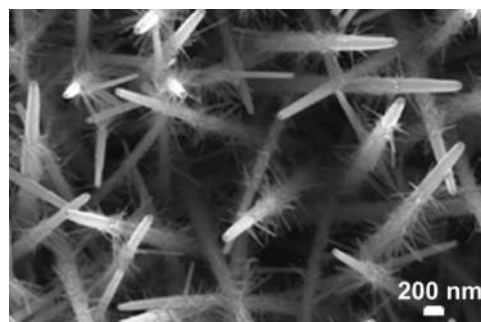

Figure 11. SEM image of branched ZnO nanowires.

greater surface to volume ratio, are able to adsorb more dye per unit thickness of the cell and thus absorb more light and collect more charge.

Despite the lower overall efficiencies, these model ZnO nanowire devices demonstrate promising fundamental improvements over the mesoporous polycrystalline films. Specifically, using the same dye, loading conditions, and electrolyte, ZnO nanowire devices showed significantly higher J_{SC} than nanoparticle films with the same dye-adsorbed surface area. Law and co-workers found that, consistent with studies on TiO_2 nanoparticle films,[129] larger ZnO nanoparticles displayed higher J_{SC} values in thin devices, presumably as a result of the higher diffusion constant in the films. In addition, the J_{SC} values of the ZnO nanowire devices were still higher, suggesting a lower series resistance within the cell.[130] Devices composed of TiO_2 nanoparticle films with the same dye-adsorbed surface area had the highest J_{SC} values. Using femtosecond transient absorption spectroscopy, Law and co-workers also found that the kinetics of charge injection from the dye excited state into the nanowires were significantly faster than across the dye—nanoparticle interface. The difference in the charge transfer rates, shown in Figure 10, may be the result of improved electron injection through the well-defined facets of the nanowire—dye interface as compared to the multitude of crystal facets presented at the nanoparticle surfaces.[127] Within the ZnO material system, the nanowire cell geometry clearly exhibits improved charge injection and transport characteristics, but the overall efficiency still lags behind TiO_2 anodes.

For nanowire-based DSSCs, the most significant limiting factor is almost always the small specific surface area (or roughness factor). Several groups have attempted to augment the area available for dye absorption in the nanowire-based cells. Tan and Wu[131] found that mixing high aspect ratio TiO_2 nanowires with TiO_2 nanoparticles in a disordered DSSC anode film improved the efficiency of the device. The DSSCs exhibited a maximum in their performance, at 20% nanowire content by weight, due to a balance between dye loading surface area and charge transport. The optimum composite mixture produced cells with an average efficiency of 8.6% as compared to 6.7% for the pure nanoparticle film. Similarly, filling the space between ZnO nanowires in vertically aligned arrays with ZnO nanoparticles improved cell performance, increasing the total surface area of the device.[132,133] Ku and co-workers found that J_{SC} increased with the addition of the nanoparticles, and the efficiency of the cell improved 3-fold, consistent with Tan and Wu's results.[132] Furthermore, the effective electron diffusion constant was about 10 times smaller than in the pure nanowire device, indicating that much of the additional photocurrent still percolated through the nanoparticle network to either the nanowire or the substrate. A subsequent study showed that improving the nanowire—nanoparticle interface using a chemical bath deposition technique further enhanced DSSC performance.[134] The cell efficiency in this case was five times greater than the pure nanowire device. Other groups have also demonstrated improved efficiencies in cells composed of ZnO nanowires grown off of the existing nanowire array.[135,136] This tree-like anode morphology, as shown in Figure 11, serves to fill the voids between nanowires with single-crystalline charge conduction pathways. If the density of these branched structures can be maximized, they should exhibit optimal solar cell performance.

The discrepancy between the properties of ZnO and TiO_2 as DSSC anode materials is the subject of ongoing investigation, but TiO_2 generally performs better with the dyes and electrolytes that have been studied. The poorer performance of the ZnO-based devices may be a result of surface chemical reactions,[137] the formation of dye aggregates,[138,139] surface trap states,[140,141] ZnO seed layer processing,[142,143] or slow charge injection from commonly used dyes.[105,144,145] To this

end, several groups have employed radial (core−shell) nanowire heterostructures to exploit the charge transfer characteristics and surface stability of TiO_2 while retaining the fast electron transport of single-crystalline nanowires. Law and co-workers[146] synthesized ZnO nanowire arrays coated by atomic layer deposition (ALD) with TiO_2 films of varying thickness. The difference between the Fermi levels of the ZnO core and TiO_2 shell creates a weak type II band offset at the interface, which provides a potential barrier to charge recombination. Overall, the core−shell devices exhibited a 2-fold improvement in efficiency (0.85−2.1%) that was attributed to a combination of improved charge injection and reduced recombination current.[147] Similar devices were constructed using SnO_2 nanowires as the conducting core with TiO_2 nanoparticle[148] and ALD-deposited[148,149] films. The nanoparticle-coated arrays gave the best device efficiencies, about 4%, and recombination time constants, as calculated from V_{OC} decay curves, were about 100-fold longer for the nanowire arrays than the nanoparticle films.

Although ZnO appears to be an inferior material to TiO_2 as the DSSC anode, model TiO_2 nanowire array structures have proved a significant synthetic challenge. Various techniques have been developed to reduce the resistance to electron transport between particles, such as growth of aligned polycrystalline nanotubes,[150−152] high-temperature sintering,[153] ordering of the mesoporous structure,[154,155] and synthesis of particle films by oriented attachment.[156] All these methods strive to minimize electronic defects at the grain boundaries, but none will likely demonstrate as great an improvement as high surface area single crystals. The decreased density of trap states leading to faster electron transport improves overall cell performance only when coupled with the energetic barrier to charge recombination provided by the nanowire structure.[100,157] Recently, several groups have achieved high-density, single-crystalline, vertically aligned TiO_2 nanowire arrays.[158,159] The efficiency of DSSCs fabricated from these arrays is encouraging, about 5%, though the nanowire density is too low such that the surface area available for dye adsorption suffers.[158] With further synthetic optimization, or perhaps combination with nanoparticles in a composite film, these TiO_2 nanowire anodes are promising candidates for high-efficiency DSSCs.

Analogous photovoltaic devices based on the principles of DSSCs have also been fabricated on ZnO nanowire substrates. Leschkies and co-workers used CdSe quantum dots, instead of an absorbing dye, to sensitize arrays of ZnO nanowires immersed in an I_2/I_3^- redox couple solution. Though the cell efficiency was low (0.4%), it had a reasonable V_{OC} of 0.6 V and an internal quantum efficiency of 50−60% over the wavelengths corresponding to the first excitonic transition of the nanoparticles.[160] Different nanoparticle sizes or compositions can be used to tune the absorption range of these cells independent of surface chemistry, unlike the sensitizing dyes. All inorganic-sensitized solar cells were fabricated on a ZnO nanowire array, with a CdSe or CdTe absorber layer, and CuSCN transparent hole-conducting layer deposited from a chemical bath solution.[161,162] The cells with the CdSe absorber layer performed better, with a 2.3% power conversion efficiency at low illumination intensities (36 mW cm^2), but both suffered from significant recombination losses.

The energy conversion efficiencies of current nanowire-based excitonic cells are not better than the best nanoparticle-based DSSCs, but the studies discussed above show that their electron transport properties are superior. Nanoparticle films have at least a 5-fold larger surface area than the best nanowire arrays, resulting in more dye loading per area of the cell and hence more absorption within the particle films. Longer or thinner nanowire arrays with comparable surface areas are a synthetic challenge, but they should improve both light absorption and charge transport within the anode.

Inorganic nanowires represent an ideal charge transport medium for nanostructured solar cells and display promising improvements over planar and nanoparticle-based devices. Further efficiency improvements may be realized in several areas of research. (1) Better synthetic control. Ideal electrode structures have not been realized, in terms of both their surface area and length as well as their band gap. (2) Improved device architectures. The performance of nanorod−polymer devices has been disappointing thus far. Incorporating different absorbers, such as small molecules or nanocrystals, and hole conductors, such as inorganic layers, in a variety of device schemes would provide comparative data to help understand the factors that determine efficiency. Atomic layer deposition is a particularly useful technique in this regard. (3) Time-dependent transport experiments. Time- and frequency-domain photocurrent and voltage experiments may shed light on the charge separation and transport properties of nanowire-based solar cell. (4) Device modeling. Three-dimensional models of nanostructured solar cells would help explain the role of electric fields and the microscopic dynamics of recombination in these cells.

5. Nanowires for Electrochemical Energy Storage

The storage of energy through electrochemical reactions is a crucial technology for portable power needs and load leveling of many alternative and conventional power sources. The proliferation of personal electronics and commercialization of electric and hybrid electric vehicles has popularized the need for rechargeable, portable power sources. High-capacity energy storage is also necessary for the widespread use of intermittent alternative energy resources, most notably from the sun and wind. For these technologies to contribute significantly to the global demand for electricity, they require efficient methods to store excess energy when it is abundant, during the day, for example, or when the wind blows, and to release it as needed. Such storage would also improve the efficiency of conventional power generation by leveling the peaks and valleys of daily energy demand.[163,164] Batteries fulfill these requirements by providing a direct route to the conversion of electrical to chemical energy.

The basis for this energy conversion is the simultaneous shuttling of electrons to and from electrodes via complementary chemical reactions. During discharge, electrons are delivered from the cathode to the anode through an electrolyte medium by spontaneous reduction and oxidation, respectively, of chemical species at the electrodes. Electrons supply power by flowing from the anode back to the cathode through an external load. Applying an opposing voltage across the cell reverses the reactions at the electrodes, thus recharging the battery capacity. Fuel cells are similar to batteries in that spontaneous redox reactions at the electrodes produce a voltage to push electrons across an external load. The reactants for these reactions, however, are generally not recycled within the cell but rather supplied to the electrodes from an external source as liquids or gases. In a hydrogen fuel cell, for example, hydrogen and oxygen gas are oxidized

and reduced at the anode and cathode, respectively, forming water, which is subsequently removed. Similarly, photoelectrochemical (PEC) cells use a photovoltage, instead of an externally applied voltage, to drive redox reactions at the electrode surfaces in a process analogous to battery charging. The DSSC devices discussed above are in fact PEC cells where the chemical fuel, the oxidized electrolyte, is converted back to an electrical potential internally. The factors affecting PEC efficiencies are therefore similar to those in the DSSC section above and will not be covered in further detail. Suffice it to say that nanowires have been used in PEC devices with some demonstrated advantages over planar and nanoparticle-based electrodes.[152,165−174]

Lithium ion batteries, which use lithium cations to transport charge between electrodes, are promising for rechargeable chemical energy storage due to the fast mobility and high energy density of lithium ions. Lithium also has a large negative reduction potential ($E^0 = -3.05$ V) which generates a high-voltage output. Only hydrogen would offer better storage and transport properties if not for the difficulty of storing large weight fractions of it.[163] The energy stored in these batteries is a result of the difference in the redox potentials of lithium insertion into the two electrodes. As a result, the battery capacity depends on the weight or volume fraction of lithium that each electrode can hold, and the rate of charging and discharging depends on the electrical resistance of the electrodes and the rate of lithium diffusion in and out of the electrode materials.[164]

Nanoparticles have been employed as electrode materials to improve cell properties in several ways. First, small diameter particles have large surface-to-volume ratios and short lithium diffusion lengths. The diffusion time varies as the square of the length, so the greater available surface area and reduction of particle sizes from micro- to nanometers result in orders of magnitude increases in lithium insertion and discharging kinetics. Nam and co-workers, for example, used viral capsid templates to nucleate monodisperse Co_3O_4 and $Au-Co_3O_4$ composite nanoparticles by a low-temperature synthesis, which exhibited superior lithium storage and discharge properties normally found only in higher temperature syntheses ($\sim$500 °C).[175] Second, nanoparticles may sustain more damaging structural changes than their bulk material counterparts. Particles below a critical size may resist phase transformations[176] or undergo transitions through and amorphous intermediate[177,178] and prevent large lattice strains resulting from phase coexistence. Furthermore, nanoparticles resist cracking due to strain relaxation at the surface[179,180] and mechanical considerations.[181] Finally, the high surface-to-volume ratio of the nanoparticle electrodes increases their reactivity significantly, which allows for different reaction mechanisms than are observed at bulk material surfaces. For example, instead of incorporating into the lattice of several metal−oxide electrode materials, lithium reversibly reduces the electrodes to metal particles surrounded by Li_xO.[182]

As with PEC or solar cells, nanoparticle battery electrodes suffer from poor charge transport. While some materials with high lithium storage capacities are inherently poor conductors, the cyclic strain fluctuations of the electrodes upon lithium insertion and removal causes greater separation between nanoparticles and impedes charge percolation to and from the current collectors. The former can be addressed with impurity doping of the electrode material, though these defects may lead to deterioration of the electrochemical

properties of the electrode. The latter problem is often remedied by encapsulating the nanoparticles in a conductive carbon matrix, thus reducing the series resistance to the current collector.[176] Carbon, however, even in the form of graphite has a limited capacity for intercalating lithium, such that a pure graphite electrode can reach a specific capacity of about 350 mAh g^{-1}.[164,183] As a result, the specific capacity of the electrode suffers. In materials such as silicon and tin the effects of volume expansion and contraction (up to 400% for $Li_{4.4}Si$) are exacerbated due to their especially high capacity for lithium.[184] For a comprehensive review of silicon nanoparticle-based anodes, see ref 185. The high lithium content of these alloys though is precisely the property that makes these materials so attractive for battery anodes.

Due to the lack of a conductive matrix, nanometer-scale thin films of amorphous silicon exhibit much greater specific capacities than nanoparticle electrodes and longer cycle lives than bulk silicon.[185] These films routinely store >3000−4000 mAh g^{-1} due to their large surface-to-volume ratio and exhibit excellent capacity retention up to several hundred cycles. For up to 200 cycles, Ohara and co-workers found that thinner amorphous silicon films had a greater specific capacity, 3700, 2900, and 2900 mAh g^{-1} for 50, 150, and 440 nm films, and that the capacity loss per cycle increased with thickness.[186,187] Their results follow this trend up to thicker films of several micrometers.[188] The researchers concluded that the improved charge retention in the thinner films was a result of less cracking and degradation of the electrical contact between the thinner films and their substrates. The thinner the films, the better they were able to withstand the expansion and contraction cycles under lithium loading. Although these results are fundamentally significant, the application of thin films in commercial battery technologies seems limited since the surface area accessible to the electrolyte is limited by the area of the substrate.

Nanowire anodes, in contrast to nanoparticle and thin film materials, should in principle maximize the electrode surface area while maintaining good electrical connections to the current collector (Figure 12). Indeed, Gao and co-workers adopted this strategy for VLS-grown silicon and germanium nanowires but with disappointing capacities of about 800−1500 mAh g^{-1} and no cycling experiments.[189] Chan and co-workers discovered they could achieve near theoretical specific capacity (4200 mAh g^{-1}) for VLS-grown silicon nanowire anodes on a stainless steel current collector.[190] The anode capacity fell immediately following the first cycle but remained constant at about 3000 mAh g^{-1} for 10 cycles at a C/20 rate (i.e., discharging 1/20th the cell capacity per hour). Another device exhibited a capacity of roughly 3500 mAh g^{-1} for 20 cycles at a C/5 rate. TEM images show that the initially single-crystalline nanowires became amorphous after lithium insertion and reverted to amorphous silicon after the first discharge cycle. Ge nanowire anodes synthesized in a similar manner exhibited analogous results, albeit at a lower specific capacity of 1141 mAh g^{-1} over 20 cycles at a C/20 rate.[191] With another variation, Cui and co-workers investigated the cycling behavior of crystalline core−amorphous shell silicon nanowire anodes also grown by the VLS mechanism.[192] Due to differences in the reduction potential of lithium in amorphous versus crystalline silicon, the researchers proposed that the core could serve as a mechanical support and provide high electrical conductivity along the entire length of the nanowire array. Indeed, the lithium reduction peaks were distinguishable in electrochemical
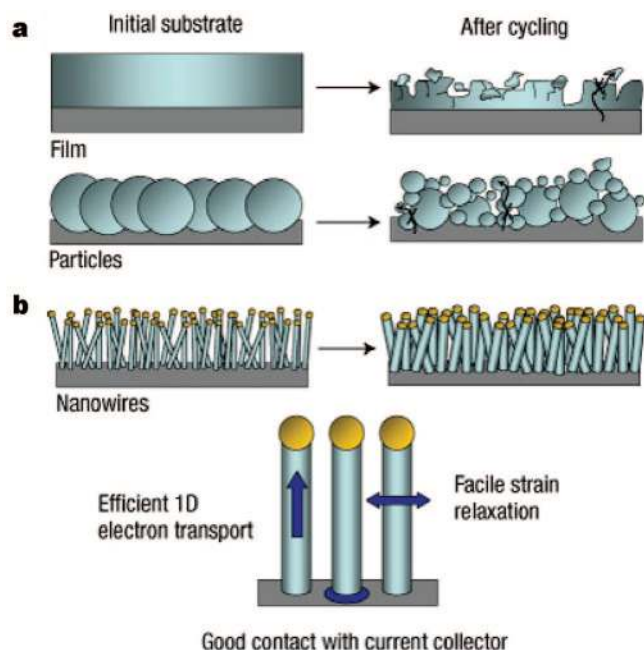
Figure 12. Schematic representation of (a) the failure mechanisms of thin film and nanoparticle silicon lithium ion battery anodes and (b) the expected mechanisms of cycling stability of silicon nanowire anodes. (Reprinted with permission from ref 190. Copyright 2008 Nature.)

potential spectroscopy scans. Although cycling below the crystalline silicon reduction potential for lithium produced a large initial specific capacity, 2400 mAh g^{-1}, the capacity dropped about 20% over 30 cycles. By cycling the cells with a lower voltage limit above this potential, the anodes exhibited lower capacities, about 800−1000 mAh g^{-1}, but lost less than 10% of their capacity over 100 cycles, making them promising candidates for practical applications.

Other nanowire-based anodes have been studied in a variety of material systems and also demonstrate improved properties as compared to nanoparticle and bulk materials. Mesoporous materials, essentially inverse nanowire structures, composed of carbon and polycrystalline silicon−carbon composites, akin to encapsulated nanoparticle systems, have demonstrated higher specific capacities and rate capabilities (the capacity upon discharge at various rates) than films or bulk electrodes.[193−195] These improvements are likely a result of the high electrode surface area, and the short lithium diffusion lengths improve the rate at which charge can be extracted from the electrode. SnO$_2$ nanowire anodes have also shown improved specific capacity for lithium insertion as compared to nanoparticle anodes and retain these high capacities even at fast discharge rates (>700 mAh g^{-1} at 8C).[196,197] Similar capacities were measured for mesoporous FeC$_2$O$_4$ nanoribbons.[198] Titania nanowires, synthesized as TiO$_2$−B, a polymorph of titania with a more open lattice structure than anatase and rutile,[199] exhibited better lithium capacity than nanoparticles in both liquid and polymer electrolyte cells.[200,201] TiO$_2$−B also has the added benefit of reducing lithium at a much higher potential than lithium metal, thus preventing growth of elemental lithium dendrites, which can short cells and lead to excessive heating and explosion, even under fast charging conditions.[201] Single- and polycrystalline Co$_3$O$_4$ nanowires have also been implemented as battery anodes with improved capacity and rate capabilities.[175,202−204] Analogous arrays of vertically aligned, electrodeposited Cu nanowires have been used as supports

for polycrystalline Fe$_3$O$_4$ shells, which produced cells with surprisingly persistent specific capacities of 800−900 mAh g^{-1} over 50 cycles and high rate capacities, retaining 75% of the discharge capacity of the C/32 rate at a 8C rate.[205]

Cathodes composed of nanowire-based materials show improved properties as well, the main difference between these and anode materials being the voltage at which they reduce lithium. The measured specific capacities and rate capability of LiMn$_2$O$_4$ nanowire and nanotube cathodes is greater than comparable nanoparticle electrodes (∼100 mAh g^{-1} at slow discharge rates).[206,207] The discharge capacity at various rates was found to improve with decreasing nanotube wall thickness, consistent with the shorter lithium diffusion lengths.[206] Furthermore, Kim and co-workers found that the nanowires retained good electronic connections to the current collector through many charge/discharge cycles. Consequently, less conductive carbon was required to preserve conductivity through the electrode, effectively increasing the specific capacity of the nanowire array to twice that of commercial nanoparticle cathodes.[207] Similar improvements were observed in C@Au@V$_2$O$_5$ core−shell−shell nanorod structures synthesized by a template method.[208] The crystallinity of V$_2$O$_5$ nanorods also aids Li intercalation, as Takahashi and co-workers discovered that nanorods grown by electrochemical deposition had 5 times greater current density than substrates with poorer crystallinity synthesized by a sol−gel method.[209,210] V$_2$O$_5 \cdot n$H$_2$O was found to be even more active for lithium incorporation, and Ni@V$_2$O$_5 \cdot n$H$_2$O core−shell nanowire arrays showed 10 times greater current density than the crystalline nanorods.[211] Somewhat conflictingly, another study found that amorphous V$_2$O$_5$ nanotube arrays also showed promising specific capacities of about 300 mAh g^{-1} but degraded by cycling to 160 mAh g^{-1}.[212] In addition to short diffusion lengths and large surface areas, the diffusion constant of lithium in V$_2$O$_5$ is sensitive to the material dimensions. Chan and co-workers determined that the diffusion of lithium in V$_2$O$_5$ was up to 1000 times faster in nanoribbons than in bulk and, moreover, that Li$_3$V$_2$O$_5$ reverted to crystalline V$_2$O$_5$ upon removal of lithium from the electrode.[213] The increased surface reactivity of the nanoribbons is presumably responsible for facilitating the phase transformations associated with lithium insertion and extraction. Of particular interest is the energy storage mechanism of these V$_2$O$_5$ nanostructured materials. Their energy density resembles that of typical batteries, while their power density is comparable to that of capacitors, another device for which nanowire electrodes are receiving increasing attention. These nanostructures clearly store chemical energy in different ways than conventional materials and represent an intriguing avenue for future research.

In short, nanowire-based materials have demonstrated significant improvements over conventional lithium battery electrode materials with higher specific capacities, rate capabilities, better cycling performance, and new phase transformation behavior. Although it is unlikely that lithium secondary batteries will be used for all applications, especially those requiring very high rate capabilities, the design principles elucidated by the study of nanowire electrodes in these cells may help develop significantly improved electrodes in other rechargeable battery systems. For example, transportation accounts for over 60% of the petroleum energy consumption in the United States and about 20% of total energy consumption worldwide.[214] Lithium ion batteries are currently used to power electric and hybrid vehicles and

could potentially provide inroads for alternative energy into these markets in place of relatively inefficient combustion engines. However, due to current limitations on the properties of electrolytes, separators, and charge collectors, specific capacities above 1000 mAh g^{-1} or energy densities above 1 Ah cm^{-3} are unlikely to significantly improve overall battery performance.[185] Looking forward, the most important advances will likely come from discovering more inexpensive and abundant materials that can achieve dense lithium storage capacities and long cycle lifetimes by altering the electrode morphology. In this sense, the promise of scalable syntheses[215] of nanowire-based anodes with long cycle lives is encouraging for future energy storage applications.

6. Nanowires for Thermoelectric Applications

Thermoelectric materials convert heat to electricity. When placed in a temperature gradient, these materials generate an electrical potential that can be used to power an external load. Conversely, passing a current through a thermoelectric material will establish a temperature gradient across the material, shunting heat from one side to the other. Consequently, depending on their temperature range of maximum efficiency, these materials may be used for either solid-state power generation or cooling. Thermoelectric modules may also be used as power cogenerators by salvaging waste heat from other power generators such as combustion engines. Approximately 90% of the world's power ($\sim 10^{13}$ W or 10 TW) is generated by heat engines that operate at 30–40% efficiency, such that roughly 15 TW of heat is lost to the environment. Thermoelectric materials may potentially convert part of this low-grade waste heat to electricity, which could result in significant fuel savings and a reduction in carbon emissions.

In a temperature gradient, charge carriers on the hot side of a material occupy higher energy electronic states than those on the cold side. These hot electrons (or holes) diffuse to the cold side, where the density of available states is greater, until the opposing electric field is sufficient to stop the flow of charge. The efficiency at which thermoelectric materials convert heat to electricity depends on the thermoelectric figure of merit (ZT), which is defined as $ZT = S^2 T / \rho k$, where S, ρ, k, and T are the Seebeck coefficient, electrical resistivity, thermal conductivity, and absolute temperature, respectively. Conceptually, ideal thermoelectric materials must have a low k, to maintain large temperature gradients, and a low ρ, to minimize Joule heating and maximize the available charge carriers contributing to the thermoelectric effect. S depends on the electronic band structure of the material near the Fermi level and varies with the change in carrier density per degree Kelvin. The total efficiency of a thermoelectric material is a function of the Carnot efficiency (the thermodynamic maximum efficiency) and ZT according to

$$\eta = \eta_C \frac{\sqrt{1 + ZT} - 1}{\sqrt{1 + ZT} + T_c / T_h}$$

In the above equation T_h and T_c are the temperature of the hot and cold sides in degrees Kelvin, respectively, and η_C is the Carnot efficiency ($\eta_C = (T_h - T_c)/(T_h)$ for power generation and $\eta_C = (T_c)/(T_h - T_c)$ for refrigeration). In this case, ZT is taken at the average temperature between the two sides. As an example, for T_h and T_c of 400 and 300K, respectively, a ZT of 1, 2, and 3 corresponds to conversion efficiencies of

approximately 20%, 30%, and 35% of Carnot, respectively. Compression engines used for refrigeration typically operate at around 30% of Carnot efficiency, so thermoelectric modules with $ZT > 2-3$ could potentially replace these with solid-state devices, which do not use compressed gases or any moving parts. Similarly, such devices could be used to salvage waste heat from automobile engines to either run hybrid electric engines or recharge batteries.

Currently, the most commonly used commercial thermoelectric material is Bi_2Te_3 and its alloys, which have $ZT \approx 1$ at room temperature. Over the past five decades, however, it has been challenging to increase ZT above 1, since the parameters of ZT are generally interdependent.[216–218] For a given material, ρ decreases with increasing charge carrier concentration but so does S, while k increases. Both electrons and lattice vibrations, called phonons, can conduct heat. As a result, k can be decomposed into two terms, k_l and k_e, which correspond to the lattice and electronic contributions to thermal conductivity, respectively. At very high carrier concentrations, such as in metals, k_e contributes significantly to the total k and reduces S significantly, thus diminishing ZT. At the other extreme, insulators generally have a low k and high S but ρ is too large for the material to exhibit a high ZT. As a general rule, ZT is maximized when the carrier concentration is about $10^{19}-10^{21}$ cm^{-3}, corresponding to highly doped semiconductors and semimetals.[216,217,219]

Mingo and Dresselhaus and co-workers predicted that dimensionally confined materials may exhibit greatly enhanced thermoelectric performance due to changes in their electronic band structure.[220–226] As ρ depends on the electronic density of states (DOS) and S depends on the energy derivative of the DOS near the Fermi energy, sharp increases in the DOS due to electronic confinement may significantly improve these parameters. Experimental results have borne out the predicted enhancement of S or the power factor (S^2/ρ) with electronic confinement in nanostructured materials, but none have demonstrated an overall improvement in ZT.[227–229] Nanowire materials have been investigated as promising materials in this respect for some time, though with mixed results. As the diameter or grain size of nanowires composed of Bi and its alloys (Se, Te, and Sb) decreases, surface scattering of electrons dominates and the transport measurements become sample dependent.[230–233] Several groups have observed enhanced Seebeck coefficients in disordered thin films of Bi alloy and PbTe nanowires and nanorods, though the characterization of these films is poor, and hence, the cause of this enhancement remains unclear.[234–239] The thermoelectric properties of individual InSb and $CrSi_2$ nanowires have also been measured and were found to suffer from similar surface effects.[240–242] In another approach, field-effect gating of thermoelectric nanowires to manipulate the DOS near the Fermi level has been predicted[243] and shown to effectively enhance S and ZT overall,[244] though not enough to improve upon state-of-the-art bulk materials. Recent experimental work on thallium-doped bulk PbTe demonstrated for the first time that increasing the density of states near the Fermi level does lead to a 2-fold increase in ZT (from 0.7 to 1.5 at 800 K), though this result is irrespective of electronic confinement.[245] Consequently, nanoscale manipulation of the electronic band structure as a means to improve the thermoelectric properties of materials is still a work in progress. The large theoretical enhancements in ZT should motivate future research in

surface passivation, through chemistry or heterostructures, to realize these predictions.

Nanostructured thermoelectric materials have shown great promise as several groups have observed ZT values of 1.5−2.5.[246−248] Electronic confinement and subsequent changes in the electronic band structure, however, are not the sources of this ZT enhancement. In these recent, high-ZT bulk nanostructured materials, the electronic properties, ρ and S, remain similar to homogeneous bulk materials. Their k, on the other hand, is significantly lower. All other material parameters being equal, this decrease in thermal conductivity is the cause of ZT enhancement in nanostructured bulk materials.[218] The nanostructures incorporated either through controlled growth methods, such as molecular beam epitaxy (MBE),[246,248] or by precipitation during crystallization[247,249] evidently play a crucial role in reducing the thermal conductivity of these materials.

Nanostructures in these materials impede the flow of heat by increasing the rate of phonon scattering. Treating phonon transport as purely diffusive, the Boltzmann transport equation gives the thermal conductivity as $k = 1/3Cvl$, which can also be expressed with frequency dependence by $k = 1/3 \int C(\omega)v(\omega)l(\omega) \, d\omega$, where $C(\omega)$, $v(\omega)$, and $l(\omega)$ are the phonon frequency-dependent heat capacity, group velocity, and mean free path, respectively. Assuming that incorporated nanostructures do not change the phonon dispersion relation, $C(\omega)$ and $v(\omega)$ will essentially be the same as in the bulk homogeneous material. $l(\omega)$, on the other hand, is proportional to the relaxation time, τ, of different phonon scattering mechanisms within the crystal lattice. For multiple simultaneous scattering processes, the scattering probabilities, related to the inverse of τ corresponding to each process (τ_1, τ_2, etc.), are additive, such that $l_{ph}^{-1}(\omega) = l_1^{-1}(\omega) + l_2^{-1}(\omega) + ...$. This relation implies that l_{ph} of a given phonon mode (i.e., frequency) will be limited by the scattering mechanism with the highest probability, i.e. the shortest l.

Keeping in mind the frequency dependence of the various relaxation times, phonon modes of different wavelengths will scatter with different probabilities by each process. For example, random atomic impurities in the lattice may scatter short wavelength phonons efficiently due to their comparable dimensions, whereas long-wavelength phonons spanning many unit cells may pass unaffected. Tailoring the dimensions of various scattering elements provides a promising approach for broadband impedance of phonon transport. Nanostructures, in particular, play a significant role in scattering phonons and can lead to thermal transport properties which significantly differ from bulk behavior.[250] Thus, by careful incorporation of atomic- and nanoscale scattering sites, novel materials may be fabricated with superior thermoelectric performance.

Point defects or impurities have long been known to impact the lattice thermal conductivity of materials.[251−253] Even isotopic impurities affect low-temperature phonon transport.[254] At very low temperatures, boundary and impurity scattering limit phonon transport. The peak thermal conductivity occurs at temperatures where high-energy modes begin to scatter by phonon−phonon interactions, called Umklapp processes. This peak typically occurs below 50 K, and temperatures above this will be referred to, generally, as "high temperatures". Umklapp scattering scales as ω^2, such that at high temperatures most of the high-frequency modes are scattered, leaving the long-wavelength modes to dominate phonon transport.[255] Generally, materials with low lattice

thermal conductivity values near room temperature are those with low symmetry, polyatomic, ionic lattices, and large mass disparities between their constituent atoms. Common examples include the lead chalcogenides, bismuth telluride and its alloys, perovskites, and spinel structures and their alloys. This mass asymmetry, along with bond anharmonicity, prevents the propagation of some of the long-wavelength modes, thus reducing the overall thermal conductivity near room temperature and above to several W m^{-1} K^{-1}. Highly symmetric, monatomic, covalent lattices of light elements, such as silicon and diamond, on the other hand, conduct heat very well, on the order of 100 and 1000 W m^{-1} K^{-1}, respectively. Consequently, long-wavelength phonons have significantly longer mean free paths in these materials. It is precisely because of this high thermal conductivity that bulk silicon is a poor thermoelectric material ($ZT = 0.01$).

Silicon has recently become an interesting material for thermoelectric research, however, due to the long mean free path of phonons that dominate heat transport in silicon at high temperature. Mid- to long-wavelength phonons are efficiently scattered at boundaries and nanoscale interfaces.[252,256] Goodson and co-workers examined the thermal conductivity of thin silicon films, down to less than 100 nm, and found significant reductions in thermal conductivity at high temperatures. In contrast to the work on layered nanostructures deposited by MBE, where layers were of the order of nanometers in thickness, Goodson and co-workers discovered that the thermal conductivity of silicon decreased in layers thinner than about a micrometer.[257,258] These findings suggest that some long-wavelength phonons propagate more than a micrometer before scattering in bulk silicon at room temperature. They estimated that the mean free path of phonons in silicon at room temperature is close to 300 nm, and films less than 100 nm thick have a thermal conductivity one-half that of bulk.[259] In contrast, electrons in highly doped silicon, i.e., with optimal electrical conductivity for thermoelectric applications, have a mean free path of 1−10 nm at room temperature.[26,260] Materials with characteristic length scales within the range of tens to hundreds of nanometers should effectively decrease thermal conductivity while maintaining bulk electronic properties. This strategy has been explicitly realized in nanocrystalline p- and n-type BiSbTe[261−263] and p- and n-type SiGe[264,265] alloys with enhanced ZT values 1.5−2 times those of the corresponding bulk materials. Similar results were obtained in LAST-type materials[249] and InGaAs[266] with the intentional inclusion of nanoscale particles into crystalline lattices. Specifically, Kim and co-workers showed that the thermal conductivity nanostructured materials could be reduced beyond the alloy limit, i.e., the lowest k achievable by point defect scattering.[266] Semiconductor nanowires, with their extensive surface area and established electrical properties, are seemingly ideal structures to exploit this length scale disparity for improved thermoelectric performance.

Indeed, silicon nanowires exhibit interesting thermal transport behavior. Majumdar and co-workers developed a method by which to directly measure the thermal conductivity of individual nanowires using microfabricated devices.[11,12,267] Two thermally isolated resistive thermometers are bridged by a single nanowire which, to a very high accuracy, is the only channel for heat conduction between them. As the temperature on one side increases, the rise in temperature on the other side is measured, and the difference between the two is used to extract the thermal conductivity
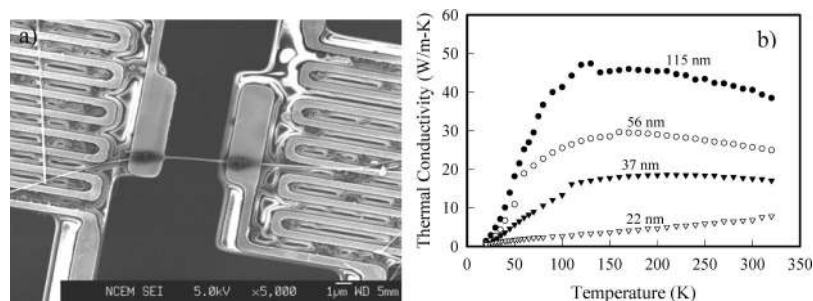
Figure 13. (a) SEM image of the microfabricated device used to measure the thermal conductivity of individual nanowires. (b) Thermal conductivities of single-crystalline pure Si nanowires vary with diameter. The number besides each curve denotes the corresponding wire diameter. (Reprinted with permission from ref 11. Copyright 2003 AIP.)
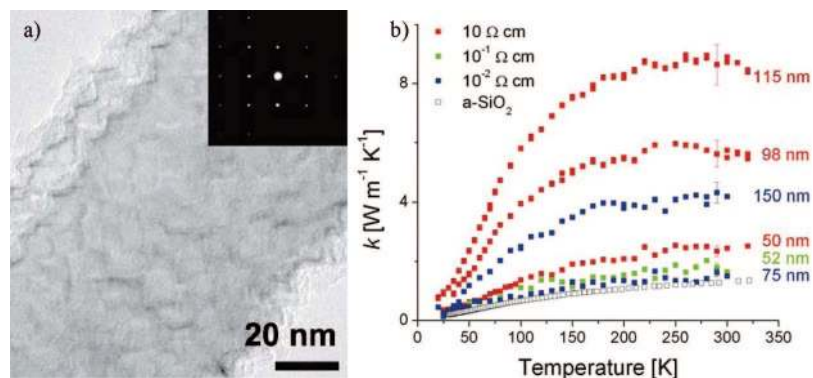

Figure 14. Rough silicon nanowires. (a) TEM image of an EE silicon nanowire and selected area electron diffraction pattern indicating the nanowire is single crystalline (inset). (b) Temperature-dependent k of EE Si nanowires etched from wafers of different resistivities: 10 (red squares), 10^{-1} (green squares; arrays doped postsynthesis to 10^{-3} Ω cm), and 10^{-2} Ω cm (blue squares). For the purpose of comparison, the k of bulk amorphous silica is plotted with open squares. The smaller highly doped EE Si nanowires have a k approaching that of insulating glass, suggesting an extremely short phonon mean free path. Error bars are shown near room temperature and should decrease with temperature. (Reprinted with permission from ref 272. Copyright 2008 Nature.)

of the nanowire. Li and co-workers found that the k values of silicon nanowires synthesized by the VLS mechanism were diameter dependent, in agreement with the thickness dependence in the thin film studies, but up to 10- to 20-fold lower than bulk at room temperature (Figure 13).[11] These results can be explained by assuming diffusive phonon scattering at the surfaces, such that the mean free path is limited by the diameter of the nanowire, $l(\omega) \approx d$.[268] Interestingly, the narrowest nanowire measured, 22 nm in diameter, exhibited an anomalous linear dependence of $k(T)$, whereas k typically varies as $\sim T^3$ in bulk at low temperatures. Further studies on small-diameter nanowires (<30 nm) found the same consistent linear dependence up to about 100 K.[269] Theoretical modeling explains this behavior as a pseudolinear temperature dependence as a result of overlap between ballistic and diffusive transport regimes. This theory suggests that phonon scattering at the nanowire surface is actually a frequency-dependent process, such that not all $l(\omega) = d$.

Incorporating nanoscale roughness on the surfaces of silicon nanowires serves to further reduce the transmission of phonons along their length. Arrays of rough nanowires have been synthesized by an electroless wafer etching technique (EE) in an aqueous solution of silver nitrate and hydrofluoric acid. The reaction proceeds by Ag^+ reduction to silver metal on the wafer surface by oxidation of the surrounding silicon lattice, which is then dissolved by HF in solution. The silver metal forms a mesh-like network which etches its way vertically into the wafer, leaving behind high aspect ratio silicon pillars.[39,270,271] The arrays etch vertically into the silicon, up to tens of micrometers, irrespective of the wafer crystallographic orientation, dopant concentration, or type. TEM analysis of the EE nanowires

reveals that they are single crystalline with rough surfaces but otherwise defect free (Figure 14a).[272]

Thermal transport measurements of these nanowires show a diameter-dependent thermal conductivity much like that of the VLS-grown nanowires but a factor of 5–10 lower at corresponding diameters (Figure 14b). The difference is greater for smaller diameter nanowires. Furthermore, the peak thermal conductivity occurs near room temperature for the EE nanowires, as compared to 150–200 K for the VLS nanowires and 25 K for bulk silicon.[272] The late onset of Umklapp scattering in the rough nanowires suggests that the nanowire surfaces scatter phonon efficiently up to high temperatures. It is possible that the roughness behaves like nanoscale particles at the surface, disrupting the lattice periodicity and leading to higher rates of diffuse or back-scattered phonon reflections. These mechanisms have been theorized to reduce thermal conductivity in silicon nano-wires[273,274] but not the extent observed for the EE nanowires. Thermal transport measurements of PbX (X = S, Se, Te) nanowires also show that the peak in thermal conductance as a function of temperature decreases in magnitude and shifts to higher temperatures, or disappears altogether, with decreasing nanowire diameter.[275]

The thermal conductivity of EE nanowires further de-creases with increasing surface roughness. To optimize the electronic properties of the nanowires for thermoelectric applications, the arrays were doped to $\sim 10^{19}$ cm^{-3} by annealing in BCl_3 vapor. The thermal conductivities of the smallest nanowires, 50–75 nm in diameter, approach 1.6 W m^{-1} K^{-1} at room temperature, a full 100-fold decrease from bulk values.[276] By subtracting the electronic contribution using the Wiedemann–Franz law, the lattice contribution
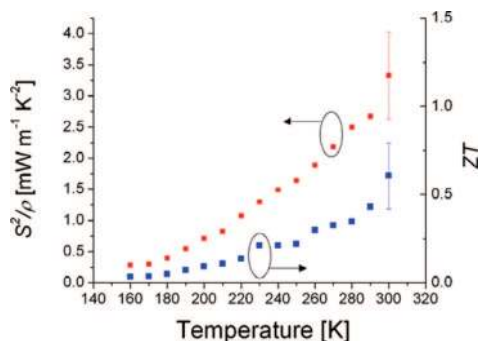
Figure 15. Single silicon nanowire power factor (red squares) of the nanowire and calculated ZT (blue squares). Reprinted with permission from ref 272. Copyright 2008 Nature.)

to thermal conductivity was calculated as ~1.2 W m^{-1} K^{-1},[260,272] which is surprisingly close to the amorphous limit for silicon and the thermal conductivity of silica at room temperature.[277,278]

That a roughly 50 nm single-crystalline nanowire conducts heat like an amorphous insulator is an unexpected result. Assuming diffusive reflections of phonons from the nanowire surface, the mean free path is limited to the nanowire diameter, and a model based on Boltzmann transport theory can explain the thermal conductivity trends in VLS-grown nanowires but grossly overestimates the values for EE nanowires.[268] On the other hand, the lattice thermal conductivity of amorphous solids can be estimated assuming the mean free path is limited to one-half the phonon wavelength due to the lack of extended coherence over a disordered lattice.[278] The nanowire channel, however, is single crystalline, and hence, there is no reason to believe phonon modes would lose coherence over a distance $l = \lambda/2$, especially considering that the diameter is about 10 times the lattice constant. Conventional models fail to describe the observed phonon transport behavior, but the comparison between VLS and EE nanowires suggests the roughness plays a significant role.

The electronic properties of individual nanowires were measured in order to assess the ZT of EE nanowires. Conventional photolithographic processing was used to pattern metal electrodes onto the dispersed nanowires. The temperature-dependent resistivity and Seebeck coefficient were both measured for each nanowire (Figure 15). For a ~50 nm EE nanowire at room temperature, the power factor, S^2/ρ, was nearly that of bulk silicon at the same dopant concentration. Since the thermal conductivity was almost 100-fold lower, ZT improved nearly 100-fold to 0.6. Though thermal data could not be gathered for thinner nanowires, electrical characterization of thinner EE nanowires suggests ZT should improve further near room temperature and surpass 1 at elevated temperatures.[272] Boukai and co-workers found similar results for lithographically defined silicon nanowires, though their ZT peaked at around 200 K.[279] The diameter of these nanowires was significantly smaller than in the previous study, 10−20 nm, and measurements of their electronic properties suggest that phonon confinement effects may enhance the Seebeck coefficient at this size scale. The measured ZT values approaching that of commercial Bi$_2$Te$_3$ demonstrate that silicon nanowires are a viable and promising thermoelectric material. Silicon is also the most abundant semiconductor and has the added advantage of a large industrial infrastructure suited to large-scale, inexpensive processing. Moreover, the robust aqueous synthesis, wafer-

scale processing, and vertical alignment of the EE nanowire arrays makes them ideal for thermoelectric module fabrication and large-scale manufacturing.

7. Concluding Remarks

Semiconductor nanowires, as a new class of nanomaterials, are currently the subject of extensive research with several thousands of papers published annually in the field. Nanowires are model systems for investigating the dependence of optical, electrical, magnetic, and mechanical properties on dimensional confinement. Going forward, they are promising as both interconnects and functional components in the fabrication of nanoscale optoelectronic and energy conversion devices.

Harvesting energy from the ambient environment provides a potentially endless source of energy, whether for increasing the efficiency of existing generation processes, charging batteries quasi-continuously, or enabling self-powered devices. Various types of ambient power can be harnessed, including solar, thermal, vibrational, fluidic, and electromagnetic energy. Nanowires, with their unique capability of bridging nanoscopic and macroscopic worlds, promise novel and efficient strategies for tapping into these energy sources, as discussed in this review. One emerging and exciting direction is their application to solar to fuel conversion. The generation of fuels by the direct conversion of light energy to chemical bonds in a single device is an attractive goal, but no such system has been demonstrated that shows the required efficiency, is sufficiently durable, or can be manufactured at a reasonable cost. This is one of the most challenging and complex problems facing chemists and physicists alike.

The direct solar-to-fuel approach is inspired by nature's photosynthetic organisms, which accomplish the conversion of carbon dioxide and water to carbohydrates in a single integrated system. The carbon-fixing scheme in nature displays crucial design features for an engineered solar-to-fuel conversion system: spatial and directional arrangement of the light-harvesting components, charge separation and transport, and conversion of the stored potential to chemicals at catalytic sites in compartmentalized spaces. To engineer efficient and durable systems for solar-to-fuel conversion, the rational design, synthesis, and assembly of the inorganic/organic/hybrid nanostructures at multiple length scales must take advantage of these concepts and structures. Semiconductor nanowires can be readily designed and synthesized to deterministically incorporate heterojunctions that promote charge separation and directional transport as well as to selectively position the different catalysts. It is, therefore, not surprising that these unique one-dimensional structures will be part of the solution to this challenging problem. The rapid pace of research in the field of one-dimensional nanostructures has been driven by the exciting scientific challenges and technological potential of these nanoscopic systems. The success of nanowire research has been, and will be, largely built on the synthetic control scientists can achieve for this class of nanostructures.

8. Acknowledgments

9. References

(1) http://www.eia.doe.gov/oiaf/ieo/index.html; US Department of Energy, 2007; Vol. 2008.
(2) Alivisatos, A. P. *Science* **1996**, *271*, 933.
(3) Law, M.; Goldberger, J.; Yang, P. D. *Annu. Rev. Mater. Res.* **2004**, *34*, 83.
(4) De Franceschi, S.; van Dam, J. A.; Bakkers, E. P. A. M.; Feiner, L. F.; Gurevich, L.; Kouwenhoven, L. P. *Appl. Phys. Lett.* **2003**, *83*, 344.
(5) Zhong, Z. H.; Fang, Y.; Lu, W.; Lieber, C. M. *Nano Lett.* **2005**, *5*, 1143.
(6) Bjork, M. T.; Thelander, C.; Hansen, A. E.; Jensen, L. E.; Larsson, M. W.; Wallenberg, L. R.; Samuelson, L. *Nano Lett.* **2004**, *4*, 1621.
(7) Bjork, M. T.; Ohlsson, B. J.; Thelander, C.; Persson, A. I.; Deppert, K.; Wallenberg, L. R.; Samuelson, L. *Appl. Phys. Lett.* **2002**, *81*, 4458.
(8) Thelander, C.; Martensson, T.; Bjork, M. T.; Ohlsson, B. J.; Larsson, M. W.; Wallenberg, L. R.; Samuelson, L. *Appl. Phys. Lett.* **2003**, *83*, 2052.
(9) Lu, W.; Xiang, J.; Timko, B. P.; Wu, Y.; Lieber, C. M. *Proc. Natl. Acad. Sci.* **2005**, *102*, 10046.
(10) Doh, Y. J.; van Dam, J. A.; Roest, A. L.; Bakkers, E.; Kouwenhoven, L. P.; De Franceschi, S. *Science* **2005**, *309*, 272.
(11) Li, D. Y.; Wu, Y. Y.; Kim, P.; Shi, L.; Yang, P. D.; Majumdar, A. *Appl. Phys. Lett.* **2003**, *83*, 2934.
(12) Li, D. Y.; Wu, Y.; Fan, R.; Yang, P. D.; Majumdar, A. *Appl. Phys. Lett.* **2003**, *83*, 3186.
(13) Green, M. A. *Solar Cells: Operating Principles, Technology, and System Applications*; Prentice-Hall: Englewood Cliffs, NJ, 1982.
(14) Hu, C.; White, R. M. *Solar Cells: From Basics to Advanced Systems*; McGraw-Hill Book Co.: New York, 1983.
(15) Green, M. A.; Keevers, M. J. *Prog. Photovoltaics* **1995**, *3*, 189.
(16) Green, M. A.; Wenham, S. R. *Appl. Phys. Lett.* **1994**, *65*, 2907.
(17) Kayes, B. M.; Atwater, H. A.; Lewis, N. S. *J. Appl. Phys.* **2005**, *97*, 114302.
(18) Kayes, B. M.; Filler, M. A.; Putnam, M. C.; Kelzenberg, M. D.; Lewis, N. S.; Atwater, H. A. *Appl. Phys. Lett.* **2007**, *91*, 103110.
(19) Kelzenberg, M. D.; Turner-Evans, D. B.; Kayes, B. M.; Filler, M. A.; Putnam, M. C.; Lewis, N. S.; Atwater, H. A. *Nano Lett.* **2008**, *8*, 710.
(20) Allen, J. E.; Hemesath, E. R.; Perea, D. E.; Lensch-Falk, J. L.; Li, Z. Y.; Yin, F.; Gass, M. H.; Wang, P.; Bleloch, A. L.; Palmer, R. E.; Lauhon, L. J. *Nat. Nanotechnol.* **2008**, *3*, 168.
(21) Mauk, M. G.; Rand, J. A.; Jonczyk, R.; Hall, R. B.; Barnett, A. M. 3rd World Conference on Photovoltaic Energy Conversion, Osaka, Japan, 2003.
(22) Lewis, N. S. *Science* **2007**, *315*, 798–801.
(23) Corathers, L. A. *Minerals Yearbook: Silicon*; U.S. Geological Survey: 2006.
(24) Buonassisi, T.; Istratov, A. A.; Marcus, M. A.; Lai, B.; Cai, Z. H.; Heald, S. M.; Weber, E. R. *Nat. Mater.* **2005**, *4*, 676.
(25) Wysocki, J. J.; Rappaport, P. *J. Appl. Phys.* **1960**, *31*, 571.
(26) Sze, S. M. *Physics of Semiconductor Devices*, 2nd ed.; Wiley: New York, 1981.
(27) Nelson, J. *The Physics of Solar Cells*; Imperial College Press: London, 2003.
(28) Hu, L.; Chen, G. *Nano Lett.* **2007**, *7*, 3249.
(29) Peng, K. Q.; Xu, Y.; Wu, Y.; Yan, Y. J.; Lee, S. T.; Zhu, J. *Small* **2005**, *1*, 1062.
(30) Stelzner, T.; Pietsch, M.; Andra, G.; Falk, F.; Ose, E.; Christiansen, S. *Nanotechnology* **2008**, *19*, 295203.
(31) Fang, H.; Li, X. D.; Song, S.; Xu, Y.; Zhu, J. *Nanotechnology* **2008**, *19*, 255703.
(32) Tsakalakos, L.; Balch, J.; Fronheiser, J.; Korevaar, B. A.; Sulima, O.; Rand, J. *Appl. Phys. Lett.* **2007**, *91*, 233117.
(33) Tang, Y. B.; Chen, Z. H.; Song, H. S.; Lee, C. S.; Cong, H. T.; Cheng, H. M.; Zhang, W. J.; Bello, I.; Lee, S. T. *Nano Lett.* **2008**, *8*, 4191.
(34) Martensson, T.; Svensson, C. P. T.; Wacaser, B. A.; Larsson, M. W.; Seifert, W.; Deppert, K.; Gustafsson, A.; Wallenberg, L. R.; Samuelson, L. *Nano Lett.* **2004**, *4*, 1987.
(35) Ertekin, E.; Greaney, P. A.; Chrzan, D. C.; Sands, T. D. *J. Appl. Phys.* **2005**, *97*, 114325.
(36) Chuang, L. C.; Moewe, M.; Chase, C.; Kobayashi, N. P.; Chang-Hasnain, C.; Crankshaw, S. *Appl. Phys. Lett.* **2007**, *90*, 043115.
(37) Tian, B. Z.; Zheng, X. L.; Kempa, T. J.; Fang, Y.; Yu, N. F.; Yu, G. H.; Huang, J. L.; Lieber, C. M. *Nature* **2007**, *449*, 885.
(38) Garnett, E. C.; Yang, P. D. *J. Am. Chem. Soc.* **2008**, *130*, 9224.
(39) Peng, K. Q.; Yan, Y. J.; Gao, S. P.; Zhu, J. *Adv. Mater.* **2002**, *14*, 1164.
(40) Cahen, D.; Hodes, G.; Gratzel, M.; Guillemoles, J. F.; Riess, I. *J. Phys. Chem B* **2000**, *104*, 2053.
(41) Gregg, B. A. *J. Phys. Chem. B* **2003**, *107*, 4688.
(42) Gledhill, S. E.; Scott, B.; Gregg, B. A. *J. Mater. Res.* **2005**, *20*, 3167.
(43) Kannan, B.; Castelino, K.; Majumdar, A. *Nano Lett.* **2003**, *3*, 1729.
(44) Peumans, P.; Yakimov, A.; Forrest, S. R. *J. Appl. Phys.* **2003**, *93*, 3693.
(45) Coakley, K. M.; McGehee, M. D. *Chem. Mater.* **2004**, *16*, 4533.
(46) Peumans, P.; Bulovic, V.; Forrest, S. R. *Appl. Phys. Lett.* **2000**, *76*, 2650.
(47) Yakimov, A.; Forrest, S. R. *Appl. Phys. Lett.* **2002**, *80*, 1667.
(48) Peumans, P.; Uchida, S.; Forrest, S. R. *Nature* **2003**, *425*, 158.
(49) Huynh, W. U.; Dittmer, J. J.; Alivisatos, A. P. *Science* **2002**, *295*, 2425.
(50) Thompson, B. C.; Frechet, J. M. J. *Angew. Chem., Int. Ed.* **2008**, *47*, 58.
(51) Yu, G.; Gao, J.; Hummelen, J. C.; Wudl, F.; Heeger, A. J. *Science* **1995**, *270*, 1789.
(52) Reyes-Reyes, M.; Kim, K.; Carroll, D. L. *Appl. Phys. Lett.* **2005**, *87*, 083506.
(53) Ma, W. L.; Yang, C. Y.; Gong, X.; Lee, K.; Heeger, A. J. *Adv. Fun. Mater.* **2005**, *15*, 1617.
(54) Snaith, H. J.; Arias, A. C.; Morteani, A. C.; Silva, C.; Friend, R. H. *Nano Lett.* **2002**, *2*, 1353.
(55) Huynh, W. U.; Dittmer, J. J.; Teclemariam, N.; Milliron, D. J.; Alivisatos, A. P.; Barnham, K. W. J. *Phys. Rev. B* **2003**, *67*, 115326.
(56) Arango, A. C.; Carter, S. A.; Brock, P. J. *Appl. Phys. Lett.* **1999**, *74*, 1698.
(57) Ravirajan, P.; Haque, S. A.; Durrant, J. R.; Poplavskyy, D.; Bradley, D. D. C.; Nelson, J. *J. Appl. Phys.* **2004**, *95*, 1473.
(58) Beek, W. J. E.; Wienk, M. M.; Kemerink, M.; Yang, X. N.; Janssen, R. A. J. *J. Phys. Chem. B* **2005**, *109*, 9505.
(59) Greenham, N. C.; Peng, X. G.; Alivisatos, A. P. *Phys. Rev. B* **1996**, *54*, 17628.
(60) Huynh, W. U.; Dittmer, J. J.; Libby, W. C.; Whiting, G. L.; Alivisatos, A. P. *Adv. Funct. Mater.* **2003**, *13*, 73.
(61) McDonald, S. A.; Konstantatos, G.; Zhang, S. G.; Cyr, P. W.; Klem, E. J. D.; Levina, L.; Sargent, E. H. *Nat. Mater.* **2005**, *4*, 138.
(62) Cui, D. H.; Xu, J.; Zhu, T.; Paradee, G.; Ashok, S.; Gerhold, M. *Appl. Phys. Lett.* **2006**, *88*, 183111.
(63) Sun, B. Q.; Greenham, N. C. *Phys. Chem. Chem. Phys.* **2006**, *8*, 3557.
(64) Quist, P. A. C.; Beek, W. J. E.; Wienk, M. M.; Janssen, R. A. J.; Savenije, T. J.; Siebbeles, L. D. A. *J. Phys. Chem. B* **2006**, *110*, 10315.
(65) Sun, B. Q.; Snaith, H. J.; Dhoot, A. S.; Westenhoff, S.; Greenham, N. C. *J. Appl. Phys.* **2005**, *97*, 014914.
(66) Brabec, C. J.; Zerza, G.; Cerullo, G.; De Silvestri, S.; Luzzati, S.; Hummelen, J. C.; Sariciftci, S. *Chem. Phys. Lett.* **2001**, *340*, 232.
(67) Pacios, R.; Nelson, J.; Bradley, D. D. C.; Virgili, T.; Lanzani, G.; Brabec, C. J. *J. Phys. Condens. Matter* **2004**, *16*, 8105.
(68) Kanai, Y.; Grossman, J. C. *Nano Lett.* **2007**, *7*, 1967.
(69) Anghel, C.; Derycke, V.; Filoramo, A.; Lenfant, S.; Giffard, B.; Vuillaume, D.; Bourgoin, J. P. *Nano Lett.* **2008**, *8*, 3619.
(70) Sun, B. Q.; Marx, E.; Greenham, N. C. *Nano Lett.* **2003**, *3*, 961.
(71) Hoppe, H.; Sariciftci, N. S. *Photoresponsive Polymers II* **2008**, *214*, 1.
(72) Oregan, B.; Gratzel, M. *Nature* **1991**, *353*, 737.
(73) Kang, Y. M.; Park, N. G.; Kim, D. *Appl. Phys. Lett.* **2005**, *86*, 113101.
(74) Williams, S. S.; Hampton, M. J.; Gowrishankar, V.; Ding, I. K.; Templeton, J. L.; Samulski, E. T.; DeSimone, J. M.; McGehee, M. D. *Chem. Mater.* **2008**, *20*, 5229.
(75) Rattanavoravipa, T.; Sagawa, T.; Yoshikawa, S. *Sol. Energy Mater. Sol. Cells* **2008**, *92*, 1445.
(76) Olson, D. C.; Shaheen, S. E.; Collins, R. T.; Ginley, D. S. *J. Phys. Chem. C* **2007**, *111*, 16670.
(77) Peiro, A. M.; Ravirajan, P.; Govender, K.; Boyle, D. S.; O'Brien, P.; Bradley, D. D. C.; Nelson, J.; Durrant, J. R. *J. Mater. Chem.* **2006**, *16*, 2088.
(78) Ravirajan, P.; Peiro, A. M.; Nazeeruddin, M. K.; Graetzel, M.; Bradley, D. D. C.; Durrant, J. R.; Nelson, J. *J. Phys. Chem. B* **2006**, *110*, 7635.
(79) Greene, L. E.; Law, M.; Yuhas, B. D.; Yang, P. D. *J. Phys. Chem. C* **2007**, *111*, 18451.
(80) Novotny, C. J.; Yu, E. T.; Yu, P. K. L. *Nano Lett.* **2008**, *8*, 775.
(81) Greene, L. E.; Law, M.; Tan, D. H.; Montano, M.; Goldberger, J.; Somorjai, G.; Yang, P. D. *Nano Lett.* **2005**, *5*, 1231.
(82) Greene, L. E.; Yuhas, B. D.; Law, M.; Zitoun, D.; Yang, P. D. *Inorg. Chem.* **2006**, *45*, 7535.

(83) Wang, G. M.; Swensen, J.; Moses, D.; Heeger, A. J. *J. Appl. Phys.* **2003**, *93*, 6137.

(84) Chirvase, D.; Chiguvare, Z.; Knipper, M.; Parisi, J.; Dyakonov, V.; Hummelen, J. C. *J. Appl. Phys.* **2003**, *93*, 3376.

(85) Kroeze, J. E.; Savenije, T. J.; Vermeulen, M. J. W.; Warman, J. M. *J. Phys. Chem. B* **2003**, *107*, 7696.

(86) Plank, N. O. V.; Snaith, H. J.; Ducati, C.; Bendall, J. S.; Schmidt-Mende, L.; Welland, M. E. *Nanotechnology* **2008**, *19*, 465603.

(87) Coakley, K. M.; Srinivasan, B. S.; Ziebarth, J. M.; Goh, C.; Liu, Y. X.; McGehee, M. D. *Adv. Funct. Mater.* **2005**, *15*, 1927.

(88) Olson, D. C.; Piris, J.; Collins, R. T.; Shaheen, S. E.; Ginley, D. S. *Thin Solid Films* **2006**, *496*, 26.

(89) Takanezawa, K.; Hirota, K.; Wei, Q. S.; Tajima, K.; Hashimoto, K. *J. Phys. Chem. C* **2007**, *111*, 7218.

(90) Takanezawa, K.; Tajima, K.; Hashimoto, K. *Appl. Phys. Lett.* **2008**, *93*, 063308.

(91) Gratzel, M. *Nature* **2001**, *414*, 338.

(92) Chiba, Y.; Islam, A.; Watanabe, Y.; Komiya, R.; Koide, N.; Han, L. Y. *Jpn. J. Appl. Phys., Part 2: Lett. Expr. Lett.* **2006**, *45*, L638.

(93) Kroon, J. M.; Bakker, N. J.; Smit, H. J. P.; Liska, P.; Thampi, K. R.; Wang, P.; Zakeeruddin, S. M.; Gratzel, M.; Hinsch, A.; Hore, S.; Wurfel, U.; Sastrawan, R.; Durrant, J. R.; Palomares, E.; Pettersson, H.; Gruszecki, T.; Walter, J.; Skupien, K.; Tulloch, G. E. *Prog. Photovoltaics* **2007**, *15*, 1.

(94) Wang, P.; Zakeeruddin, S. M.; Moser, J. E.; Nazeeruddin, M. K.; Sekiguchi, T.; Gratzel, M. *Nat. Mater.* **2003**, *2*, 402.

(95) Rensmo, H.; Keis, K.; Lindstrom, H.; Sodergren, S.; Solbrand, A.; Hagfeldt, A.; Lindquist, S. E.; Wang, L. N.; Muhammed, M. *J. Phys. Chem. B* **1997**, *101*, 2598.

(96) Tennakone, K.; Kumara, G. R. R. A.; Kottegoda, I. R. M.; Perera, V. P. S. *Chem. Commun.* **1999**, 15.

(97) Keis, K.; Magnusson, E.; Lindstrom, H.; Lindquist, S. E.; Hagfeldt, A. *Sol. Energy Mater. Sol. Cells* **2002**, *73*, 51.

(98) Solbrand, A.; Keis, K.; Sodergren, S.; Lindstrom, H.; Lindquist, S. E.; Hagfeldt, A. *Sol. Energy Mater. Sol. Cells* **2000**, *60*, 181.

(99) Fisher, A. C.; Peter, L. M.; Ponomarev, E. A.; Walker, A. B.; Wijayantha, K. G. U. *J. Phys. Chem. B* **2000**, *104*, 949.

(100) Green, A. N. M.; Palomares, E.; Haque, S. A.; Kroon, J. M.; Durrant, J. R. *J. Phys. Chem. B* **2005**, *109*, 12525.

(101) Rensmo, H.; Lindstrom, H.; Sodergren, S.; Willstedt, A. K.; Solbrand, A.; Hagfeldt, A.; Lindquist, S. E. *J. Electrochem. Soc.* **1996**, *143*, 3173.

(102) Lindstrom, H.; Rensmo, H.; Sodergren, S.; Solbrand, A.; Lindquist, S. E. *J. Phys. Chem.* **1996**, *100*, 3084.

(103) Sodergren, S.; Hagfeldt, A.; Olsson, J.; Lindquist, S. E. *J. Phys. Chem.* **1994**, *98*, 5552.

(104) van de Lagemaat, J.; Park, N. G.; Frank, A. J. *J. Phys. Chem. B* **2000**, *104*, 2044.

(105) Oekermann, T.; Zhang, D.; Yoshida, T.; Minoura, H. *J. Phys. Chem. B* **2004**, *108*, 2227.

(106) Nelson, J. *Phys. Rev. B* **1999**, *59*, 15374.

(107) van de Lagemaat, J.; Frank, A. J. *J. Phys. Chem. B* **2001**, *105*, 11194.

(108) Kopidakis, N.; Schiff, E. A.; Park, N. G.; van de Lagemaat, J.; Frank, A. J. *J. Phys. Chem. B* **2000**, *104*, 3930.

(109) Noack, V.; Weller, H.; Eychmuller, A. *J. Phys. Chem. B* **2002**, *106*, 8514.

(110) Galoppini, E.; Rochford, J.; Chen, H. H.; Saraf, G.; Lu, Y. C.; Hagfeldt, A.; Boschloo, G. *J. Phys. Chem. B* **2006**, *110*, 16159.

(111) Enache-Pommer, E.; Boercker, J. E.; Aydil, E. S. *Appl. Phys. Lett.* **2007**, *91*, 123116.

(112) Wang, Q.; Moser, J. E.; Gratzel, M. *J. Phys. Chem. B* **2005**, *109*, 14945.

(113) Adachi, M.; Sakamoto, M.; Jiu, J. T.; Ogata, Y.; Isoda, S. *J. Phys. Chem. B* **2006**, *110*, 13872.

(114) Kavan, L.; Gratzel, M.; Gilbert, S. E.; Klemenz, C.; Scheel, H. J. *J. Am. Chem. Soc.* **1996**, *118*, 6716.

(115) Wagner, P.; Helbig, R. *J. Phys. Chem. Solids* **1974**, *35*, 327.

(116) Nazeeruddin, M. K.; Pechy, P.; Renouard, T.; Zakeeruddin, S. M.; Humphry-Baker, R.; Comte, P.; Liska, P.; Cevey, L.; Costa, E.; Shklover, V.; Spiccia, L.; Deacon, G. B.; Bignozzi, C. A.; Gratzel, M. *J. Am. Chem. Soc.* **2001**, *123*, 1613.

(117) Nakade, S.; Matsuda, M.; Kambe, S.; Saito, Y.; Kitamura, T.; Sakata, T.; Wada, Y.; Mori, H.; Yanagida, S. *J. Phys. Chem. B* **2002**, *106*, 10004.

(118) Robertson, N. *Angew. Chem., Int. Ed.* **2006**, *45*, 2338.

(119) Renouard, T.; Fallahpour, R. A.; Nazeeruddin, M. K.; Humphry-Baker, R.; Gorelsky, S. I.; Lever, A. B. P.; Gratzel, M. *Inorg. Chem.* **2002**, *41*, 367.

(120) Hara, K.; Kurashige, M.; Dan-oh, Y.; Kasada, C.; Shinpo, A.; Suga, S.; Sayama, K.; Arakawa, H. *New J. Chem.* **2003**, *27*, 783.

(121) Fan, S. H.; Wang, K. Z. *Chin. J. Inorg. Chem.* **2008**, *24*, 1206.

(122) Bai, Y.; Cao, Y. M.; Zhang, J.; Wang, M.; Li, R. Z.; Wang, P.; Zakeeruddin, S. M.; Gratzel, M. *Nat. Mater.* **2008**, *7*, 626.

(123) Gorlov, M.; Kloo, L. *Dalton Trans.* **2008**, 2655.

(124) Kron, G.; Egerter, T.; Werner, J. H.; Rau, U. *J. Phys. Chem. B* **2003**, *107*, 3556.

(125) Thomas, D. G.; Lander, J. J. *J. Chem. Phys.* **1956**, *25*, 1136.

(126) Greene, L. E.; Law, M.; Goldberger, J.; Kim, F.; Johnson, J. C.; Zhang, Y. F.; Saykally, R. J.; Yang, P. D. *Angew. Chem., Int. Ed.* **2003**, *42*, 3031.

(127) Law, M.; Greene, L. E.; Johnson, J. C.; Saykally, R.; Yang, P. D. *Nat. Mater.* **2005**, *4*, 455.

(128) Baxter, J. B.; Aydil, E. S. *Appl. Phys. Lett.* **2005**, *86*, 053114.

(129) Nakade, S.; Saito, Y.; Kubo, W.; Kitamura, T.; Wada, Y.; Yanagida, S. *J. Phys. Chem. B* **2003**, *107*, 8607.

(130) Schumacher, J. O.; Wettling, W. In *Clean Electricity from Photo-voltaics*; Archer, M. D., Hill, R., Eds.; Imperial College Press: London, 2001.

(131) Tan, B.; Wu, Y. Y. *J. Phys. Chem. B* **2006**, *110*, 15932.

(132) Ku, C. H.; Wu, J. J. *Appl. Phys. Lett.* **2007**, *91*, 093117.

(133) Jiang, C. Y.; Sun, X. W.; Tan, K. W.; Lo, G. Q.; Kyaw, A. K. K.; Kwong, D. L. *Appl. Phys. Lett.* **2008**, *92*, 143101.

(134) Ku, C. H.; Wu, J. J. *Nanotechnology* **2007**, *18*, 505706.

(135) Suh, D. I.; Lee, S. Y.; Kim, T. H.; Chun, J. M.; Suh, E. K.; Yang, O. B.; Lee, S. K. *Chem. Phys. Lett.* **2007**, *442*, 348–353.

(136) Baxter, J. B.; Walker, A. M.; van Ommering, K.; Aydil, E. S. *Nanotechnology* **2006**, *17*, S304.

(137) Horiuchi, H.; Katoh, R.; Hara, K.; Yanagida, M.; Murata, S.; Arakawa, H.; Tachiya, M. *J. Phys. Chem. B* **2003**, *107*, 2570.

(138) Keis, K.; Lindgren, J.; Lindquist, S. E.; Hagfeldt, A. *Langmuir* **2000**, *16*, 4688.

(139) Oekermann, T.; Yoshida, T.; Minoura, H.; Wijayantha, K. G. U.; Peter, L. M. *J. Phys. Chem. B* **2004**, *108*, 8364.

(140) Liao, Z. M.; Xu, J.; Zhang, J. M.; Yu, D. P. *Appl. Phys. Lett.* **2008**, *93*, 023111.

(141) Goldberger, J.; Sirbuly, D. J.; Law, M.; Yang, P. *J. Phys. Chem. B* **2005**, *109*, 9.

(142) Elias, J.; Tena-Zaera, R.; Levy-Clement, C. *Thin Solid Films* **2007**, *515*, 8553.

(143) Noh, J. H.; Lee, S. H.; Lee, S.; Jung, H. S. *Electron. Mater. Lett.* **2008**, *4*, 71.

(144) Redmond, G.; Fitzmaurice, D.; Graetzel, M. *Chem. Mater.* **1994**, *6*, 686.

(145) Wu, J. J.; Chen, G. R.; Yang, H. H.; Ku, C. H.; Lai, J. Y. *Appl. Phys. Lett.* **2007**, *90*, 213109.

(146) Law, M.; Greene, L. E.; Radenovic, A.; Kuykendall, T.; Liphardt, J.; Yang, P. D. *J. Phys. Chem. B* **2006**, *110*, 22652.

(147) Palomares, E.; Clifford, J. N.; Haque, S. A.; Lutz, T.; Durrant, J. R. *J. Am. Chem. Soc.* **2003**, *125*, 475.

(148) Gubbala, S.; Chakrapani, V.; Kumar, V.; Sunkara, M. K. *Adv. Funct. Mater.* **2008**, *18*, 2411.

(149) Joanni, E.; Savu, R.; Goes, M. D.; Bueno, P. R.; de Freitas, J. N.; Nogueira, A. F.; Longo, E.; Varela, J. A. *Scr. Mater.* **2007**, *57*, 277.

(150) Mor, G. K.; Shankar, K.; Paulose, M.; Varghese, O. K.; Grimes, C. A. *Nano Lett.* **2006**, *6*, 215.

(151) Zhu, K.; Vinzant, T. B.; Neale, N. R.; Frank, A. J. *Nano Lett.* **2007**, *7*, 3739.

(152) Grimes, C. A.; Varghese, O. K.; Ranjan, S. *Light, Water, Hydrogen: The Solar Generation of Hydrogen by Water Photolysis*; Springer: New York, 2008.

(153) Hou, K.; Tian, B. Z.; Li, F. Y.; Bian, Z. Q.; Zhao, D. Y.; Huang, C. H. *J. Mater. Chem.* **2005**, *15*, 2414.

(154) Zukalova, M.; Zukal, A.; Kavan, L.; Nazeeruddin, M. K.; Liska, P.; Gratzel, M. *Nano Lett.* **2005**, *5*, 1789.

(155) Zukalova, M.; Prochazka, J.; Zukal, A.; Yum, J. H.; Kavan, L. *Inorg. Chim. Acta* **2008**, *361*, 656.

(156) Adachi, M.; Murata, Y.; Takao, J.; Jiu, J. T.; Sakamoto, M.; Wang, F. M. *J. Am. Chem. Soc.* **2004**, *126*, 14943.

(157) Kopidakis, N.; Benkstein, K. D.; van de Lagemaat, J.; Frank, A. J. *J. Phys. Chem. B* **2003**, *107*, 11307.

(158) Feng, X. J.; Shankar, K.; Varghese, O. K.; Paulose, M.; Latempa, T. J.; Grimes, C. A. *Nano Lett.* **2008**, *8*, 3781.

(159) Liu, B.; Boercker, J. E.; Aydil, E. S. *Nanotechnology* **2008**, *19*, 505604.

(160) Leschkies, K. S.; Divakar, R.; Basu, J.; Enache-Pommer, E.; Boercker, J. E.; Carter, C. B.; Kortshagen, U. R.; Norris, D. J.; Aydil, E. S. *Nano Lett.* **2007**, *7*, 1793.

(161) Levy-Clement, C.; Tena-Zaera, R.; Ryan, M. A.; Katty, A.; Hodes, G. *Adv. Mater.* **2005**, *17*, 1512.

(162) Tena-Zaera, R.; Katty, A.; Bastide, S.; Levy-Clement, C.; O'Regan, B.; Munoz-Sanjose, V. *Thin Solid Films* **2005**, *483*, 372.

(163) Whittingham, M. S. *MRS Bull.* **2008**, *33*, 411.

(164) Linden, D. *Handbook of Batteries*, 1st ed.; McGraw-Hill: New York, 1995.

(165) Ahn, K. S.; Shet, S.; Deutsch, T.; Jiang, C. S.; Yan, Y. F.; Al-Jassim, M.; Turner, J. *J. Power Sources* **2008**, *176*, 387.

(166) Goodey, A. P.; Eichfeld, S. M.; Lew, K. K.; Redwing, J. M.; Mallouk, T. E. *J. Am. Chem. Soc.* **2007**, *129*, 12344.

(167) Guo, M.; Diao, P.; Cai, S. M. *Appl. Surf. Sci.* **2005**, *249*, 71.

(168) Khan, S. U. M.; Sultana, T. *Sol. Energy Mater. Sol. Cells* **2003**, *76*, 211.

(169) Maiolo, J. R.; Kayes, B. M.; Filler, M. A.; Putnam, M. C.; Kelzenberg, M. D.; Atwater, H. A.; Lewis, N. S. *J. Am. Chem. Soc.* **2007**, *129*, 12346.

(170) Peng, K. Q.; Wang, X.; Lee, S. T. *Appl. Phys. Lett.* **2008**, *92*, 163103.

(171) Schierhorn, M.; Boettcher, S. W.; Ivanovskaya, A.; Norvell, E.; Sherman, J. B.; Stucky, G. D.; Moskovits, M. *J. Phys. Chem. C* **2008**, *112*, 8516.

(172) Spurgeon, J. M.; Atwater, H. A.; Lewis, N. S. *J. Phys. Chem. C* **2008**, *112*, 6186.

(173) Yang, S. F.; Wen, X. G.; Zhang, W. X.; Yang, S. H. *J. Electrochem. Soc.* **2005**, *152*, G220.

(174) Wang, R. Y.; Feser, J. P.; Lee, J. S.; Talapin, D. V.; Segalman, R.; Majumdar, A. *Nano Lett.* **2008**, *8*, 2283.

(175) Nam, K. T.; Kim, D. W.; Yoo, P. J.; Chiang, C. Y.; Meethong, N.; Hammond, P. T.; Chiang, Y. M.; Belcher, A. M. *Science* **2006**, *312*, 885.

(176) Guo, Y. G.; Hu, J. S.; Wan, L. J. *Adv. Mater.* **2008**, *20*, 2878.

(177) Meethong, N.; Huang, H. Y. S.; Carter, W. C.; Chiang, Y. M. *Electrochem. Solid State Lett.* **2007**, *10*, A134.

(178) Meethong, N.; Kao, Y. H.; Tang, M.; Huang, H. Y.; Carter, W. C.; Chiang, Y. M. *Chem. Mater.* **2008**, *20*, 6189.

(179) Yang, J.; Winter, M.; Besenhard, J. O. *Solid State Ionics* **1996**, *90*, 281.

(180) Cheng, Y. T.; Verbrugge, M. W. *J. Appl. Phys.* **2008**, *104*, 083521.

(181) Huggins, R. A.; Nix, W. D. *Ionics* **2000**, *6*, 57.

(182) Poizot, P.; Laruelle, S.; Grugeon, S.; Dupont, L.; Tarascon, J. M. *Nature* **2000**, *407*, 496.

(183) Whittingham, M. S. *Dalton Trans.* **2008**, 5424.

(184) Ryu, J. H.; Kim, J. W.; Sung, Y. E.; Oh, S. M. *Electrochem. Solid State Lett.* **2004**, *7*, A306.

(185) Kasavajjula, U.; Wang, C. S.; Appleby, A. J. *J. Power Sources* **2007**, *163*, 1003.

(186) Ohara, S.; Suzuki, J.; Sekine, K.; Takamura, T. *J. Power Sources* **2004**, *136*, 303.

(187) Takamura, T.; Ohara, S.; Uehara, M.; Suzuki, J.; Sekine, K. *J. Power Sources* **2004**, *129*, 96.

(188) Uehara, M.; Suzuki, J.; Tamura, K.; Sekine, K.; Takamura, T. *J. Power Sources* **2005**, *146*, 441.

(189) Gao, B.; Sinha, S.; Fleming, L.; Zhou, O. *Adv. Mater.* **2001**, *13*, 816.

(190) Chan, C. K.; Peng, H. L.; Liu, G.; McIlwrath, K.; Zhang, X. F.; Huggins, R. A.; Cui, Y. *Nat. Nanotechnol.* **2008**, *3*, 31.

(191) Chan, C. K.; Zhang, X. F.; Cui, Y. *Nano Lett.* **2008**, *8*, 307.

(192) Cui, L. F.; Ruffo, R.; Chan, C. K.; Peng, H. L.; Cui, Y. *Nano Lett.* **2009**, *9*, 491.

(193) Kim, H.; Cho, J. *Nano Lett.* **2008**, *8*, 3688.

(194) Kim, H.; Han, B.; Choo, J.; Cho, J. *Angew. Chem., Int. Ed.* **2008**, *47*, 10151.

(195) Li, N. C.; Mitchell, D. T.; Lee, K. P.; Martin, C. R. *J. Electrochem. Soc.* **2003**, *150*, A979.

(196) Li, N. C.; Martin, C. R. *J. Electrochem. Soc.* **2001**, *148*, A164.

(197) Park, M. S.; Wang, G. X.; Kang, Y. M.; Wexler, D.; Dou, S. X.; Liu, H. K. *Angew. Chem., Int. Ed.* **2007**, *46*, 750.

(198) Aragon, M. J.; Leon, B.; Vicente, C. P.; Tirado, J. L. *Inorg. Chem.* **2008**, *47*, 10366.

(199) Armstrong, A. R.; Armstrong, G.; Canales, J.; Bruce, P. G. *Angew. Chem., Int. Ed.* **2004**, *43*, 2286.

(200) Armstrong, A. R.; Armstrong, G.; Canales, J.; Garcia, R.; Bruce, P. G. *Adv. Mater.* **2005**, *17*, 862.

(201) Armstrong, G.; Armstrong, A. R.; Bruce, P. G.; Reale, P.; Scrosati, B. *Adv. Mater.* **2006**, *18*, 2597.

(202) Li, Y. G.; Tan, B.; Wu, Y. Y. *Nano Lett.* **2008**, *8*, 265.

(203) Lou, X. W.; Deng, D.; Lee, J. Y.; Feng, J.; Archer, L. A. *Adv. Mater.* **2008**, *20*, 258.

(204) Shaju, K. M.; Jiao, F.; Debart, A.; Bruce, P. G. *Phys. Chem. Chem. Phys.* **2007**, *9*, 1837.

(205) Taberna, L.; Mitra, S.; Poizot, P.; Simon, P.; Tarascon, J. M. *Nat. Mater.* **2006**, *5*, 567.

(206) Li, N. C.; Patrissi, C. J.; Che, G. L.; Martin, C. R. *J. Electrochem. Soc.* **2000**, *147*, 2044.

(207) Kim, D. K.; Muralidharan, P.; Lee, H. W.; Ruffo, R.; Yang, Y.; Chan, C. K.; Peng, H.; Huggins, R. A.; Cui, Y. *Nano Lett.* **2008**, *8*, 3948.

(208) Ahn, H. J.; Nam, S. H.; Lee, S. H.; Shim, H. S.; Kim, W. B. *Appl. Phys. Lett.* **2008**, *93*, 103104.

(209) Takahashi, K.; Limmer, S. J.; Wang, Y.; Cao, G. Z. *J. Phys. Chem. B* **2004**, *108*, 9795.

(210) Takahashi, K.; Wang, Y.; Cao, G. Z. *Appl. Phys. Lett.* **2005**, *86*, 053102.

(211) Takahashi, K.; Wang, Y.; Cao, G. Z. *J. Phys. Chem. B* **2005**, *109*, 48.

(212) Wang, Y.; Takahashi, K.; Shang, H. M.; Cao, G. Z. *J. Phys. Chem. B* **2005**, *109*, 3085.

(213) Chan, C. K.; Peng, H. L.; Twesten, R. D.; Jarausch, K.; Zhang, X. F.; Cui, Y. *Nano Lett.* **2007**, *7*, 490.

(214) http://www.eia.doe.gov/oiaf/ieo/index.html; US Department of Energy, 2008.

(215) Peng, K.; Jie, J.; Zhang, W.; Lee, S. T. *Appl. Phys. Lett.* **2008**, *93*, 033105.

(216) Heikes, R. R.; Ure, R. W. *Thermoelectricity: Science and Engineering*; Interscience Publishers: New York, 1961.

(217) Rowe, D. M. *CRC Handbook of Thermoelectricity*; CRC Press LLC: Boca Raton, 1995.

(218) Majumdar, A. *Science* **2004**, *303*, 777.

(219) Snyder, G. J.; Toberer, E. S. *Nat. Mater.* **2008**, *7*, 105.

(220) Hicks, L. D.; Dresselhaus, M. S. *Phys. Rev. B* **1993**, *47*, 12727.

(221) Hicks, L. D.; Dresselhaus, M. S. *Phys. Rev. B* **1993**, *47*, 16631.

(222) Lin, Y. M.; Dresselhaus, M. S. *Phys. Rev. B* **2003**, *68*, 075304.

(223) Humphrey, T. E.; Linke, H. *Phys. Rev. Lett.* **2005**, *94*, 096601.

(224) Rabina, O.; Lin, Y. M.; Dresselhaus, M. S. *Appl. Phys. Lett.* **2001**, *79*, 81.

(225) Mingo, N. *Appl. Phys. Lett.* **2004**, *85*, 5986.

(226) Mingo, N. *Appl. Phys. Lett.* **2004**, *84*, 2652.

(227) Hicks, L. D.; Harman, T. C.; Sun, X.; Dresselhaus, M. S. *Phys. Rev. B* **1996**, *53*, 10493.

(228) Lin, Y. M.; Rabin, O.; Cronin, S. B.; Ying, J. Y.; Dresselhaus, M. S. *Appl. Phys. Lett.* **2002**, *81*, 2403.

(229) Ohta, H.; Kim, S.; Mune, Y.; Mizoguchi, T.; Nomura, K.; Ohta, S.; Nomura, T.; Nakanishi, Y.; Ikuhara, Y.; Hirano, M.; Hosono, H.; Koumoto, K. *Nat. Mater.* **2007**, *6*, 129.

(230) Boukai, A.; Xu, K.; Heath, J. R. *Adv. Mater.* **2006**, *18*, 864.

(231) Grozav, A. D.; Condrea, E. *J. Phys. Condens. Matter* **2004**, *16*, 6507.

(232) Heremans, J. P.; Thrush, C. M.; Morelli, D. T.; Wu, M. C. *Phys. Rev. Lett.* **2002**, *88*, 216801.

(233) Zhou, J. H.; Jin, C. G.; Seol, J. H.; Li, X. G.; Shi, L. *Appl. Phys. Lett.* **2005**, *87*, 133109.

(234) Liufu, S. C.; Chen, L. D.; Yao, Q.; Wang, C. F. *Appl. Phys. Lett.* **2007**, *90*, 112106.

(235) Qiu, X. F.; Austin, L. N.; Muscarella, P. A.; Dyck, J. S.; Burda, C. *Angew. Chem., Int. Ed.* **2006**, *45*, 5656.

(236) Tai, G.; Zhou, B.; Guo, W. L. *J. Phys. Chem. C* **2008**, *112*, 11314.

(237) Tai, G. A.; Guo, W. L.; Zhang, Z. H. *Cryst. Growth Des.* **2008**, *8*, 2906.

(238) Zhang, G. Q.; Wang, W.; Li, X. G. *Adv. Mater.* **2008**, *20*, 3654.

(239) Yan, Q. Y.; Chen, H.; Zhou, W. W.; Hng, H. H.; Boey, F. Y. C.; Ma, J. *Chem. Mater.* **2008**, *20*, 6298.

(240) Zhou, F.; Szczech, J.; Pettes, M. T.; Moore, A. L.; Jin, S.; Shi, L. *Nano Lett.* **2007**, *7*, 1649.

(241) Seol, J. H.; Moore, A. L.; Saha, S. K.; Zhou, F.; Shi, L.; Ye, Q. L.; Scheffler, R.; Mingo, N.; Yamada, T. *J. Appl. Phys.* **2007**, *101*, 023706.

(242) Zhou, F.; Seol, J. H.; Moore, A. L.; Shi, L.; Ye, Q. L.; Scheffler, R. *J. Phys. Condens. Matter* **2006**, *18*, 9651.

(243) Kantser, V. G.; Bejenari, I. M.; Meglei, D. F. *Mater. Sci. Eng., C* **2006**, *26*, 1175.

(244) Liang, W. J.; Hochbaum, A. I.; Fardy, M.; Rabin, O.; Zhang, M. J.; Yang, P. D. *Nano Lett.* **2009**, *9*, 1689.

(245) Heremans, J. P.; Jovovic, V.; Toberer, E. S.; Saramat, A.; Kurosaki, K.; Charoenphakdee, A.; Yamanaka, S.; Snyder, G. J. *Science* **2008**, *321*, 554.

(246) Harman, T. C.; Taylor, P. J.; Walsh, M. P.; LaForge, B. E. *Science* **2002**, *297*, 2229.

(247) Hsu, K. F.; Loo, S.; Guo, F.; Chen, W.; Dyck, J. S.; Uher, C.; Hogan, T.; Polychroniadis, E. K.; Kanatzidis, M. G. *Science* **2004**, *303*, 818.

(248) Venkatasubramanian, R.; Siivola, E.; Colpitts, T.; O'Quinn, B. *Nature* **2001**, *413*, 597.

(249) Androulakis, J.; Hsu, K. F.; Pcionek, R.; Kong, H.; Uher, C.; DAngelo, J. J.; Downey, A.; Hogan, T.; Kanatzidis, M. G. *Adv. Mater.* **2006**, *18*, 1170.

(250) Chen, G. *Phys. Rev. B* **1998**, *57*, 14958.

(251) Brinson, M. E.; Dunstan, W. *J. Phys., Part C: Solid State Phys.* **1970**, *3*, 483.

(252) Cahill, D. G.; Ford, W. K.; Goodson, K. E.; Mahan, G. D.; Majumdar, A.; Maris, H. J.; Merlin, R.; Phillpot, S. R. *J. Appl. Phys.* **2003**, *93*, 793.

(253) Weber, L.; Gmelin, E. *Appl. Phys. A: Mater. Sci. Proc.* **1991**, *53*, 136.

(254) Ruf, T.; Henn, R. W.; Asen-Palmer, M.; Gmelin, E.; Cardona, M.; Pohl, H. J.; Devyatych, G. G.; Sennikov, P. G. *Solid State Commun.* **2000**, *115*, 243.

(255) Nolas, G. S.; Sharp, J.; Goldsmid, H. J. *Thermoelectrics: Basic Principles and New Materials Developments*; Springer: Berlin, 2001.

(256) Cahill, D. G.; Goodson, K.; Majumdar, A. *J. Heat Transfer: Trans. ASME* **2002**, *124*, 223.

(257) Asheghi, M.; Leung, Y. K.; Wong, S. S.; Goodson, K. E. *Appl. Phys. Lett.* **1997**, *71*, 1798.

(258) Asheghi, M.; Touzelbaev, M. N.; Goodson, K. E.; Leung, Y. K.; Wong, S. S. *J. Heat Transfer: Trans. ASME* **1998**, *120*, 30.

(259) Ju, Y. S.; Goodson, K. E. *Appl. Phys. Lett.* **1999**, *74*, 3005.

(260) Ashcroft, N. W.; Mermin, N. D. *Solid State Physics*; Saunders College Publishers: Fort Worth, TX, 1976.

(261) Poudel, B.; Hao, Q.; Ma, Y.; Lan, Y. C.; Minnich, A.; Yu, B.; Yan, X.; Wang, D. Z.; Muto, A.; Vashaee, D.; Chen, X. Y.; Liu, J. M.; Dresselhaus, M. S.; Chen, G.; Ren, Z. *Science* **2008**, *320*, 634.

(262) Cao, Y. Q.; Zhu, T. J.; Zhao, X. B.; Zhang, X. B.; Tu, J. P. *Appl. Phys. A: Mater. Sci. Process.* **2008**, *92*, 321.

(263) Zhao, X. B.; Ji, X. H.; Zhang, Y. H.; Zhu, T. J.; Tu, J. P.; Zhang, X. B. *Appl. Phys. Lett.* **2005**, *86*, 062111.

(264) Joshi, G.; Lee, H.; Lan, Y. C.; Wang, X. W.; Zhu, G. H.; Wang, D. Z.; Gould, R. W.; Cuff, D. C.; Tang, M. Y.; Dresselhaus, M. S.; Chen, G.; Ren, Z. F. *Nano Lett.* **2008**, *8*, 4670.

(265) Wang, X. W.; Lee, H.; Lan, Y. C.; Zhu, G. H.; Joshi, G.; Wang, D. Z.; Yang, J.; Muto, A. J.; Tang, M. Y.; Klatsky, J.; Song, S.; Dresselhaus, M. S.; Chen, G.; Ren, Z. F. *Appl. Phys. Lett.* **2008**, *93*, 193121.

(266) Kim, W.; Zide, J.; Gossard, A.; Klenov, D.; Stemmer, S.; Shakouri, A.; Majumdar, A. *Phys. Rev. Lett.* **2006**, *96*, 045901.

(267) Shi, L.; Li, D. Y.; Yu, C. H.; Jang, W. Y.; Kim, D. Y.; Yao, Z.; Kim, P.; Majumdar, A. *J. Heat Transfer: Trans. ASME* **2003**, *125*, 1209.

(268) Mingo, N.; Yang, L.; Li, D.; Majumdar, A. *Nano Lett.* **2003**, *3*, 1713.

(269) Chen, R.; Hochbaum, A. I.; Murphy, P.; Moore, J.; Yang, P. D.; Majumdar, A. *Phys. Rev. Lett.* **2008**, *101*, 105501.

(270) Peng, K. Q.; Wu, Y.; Fang, H.; Zhong, X. Y.; Xu, Y.; Zhu, J. *Angew. Chem., Int. Ed.* **2005**, *44*, 2737.

(271) Peng, K. Q.; Yan, Y. J.; Gao, S. P.; Zhu, J. *Adv. Funct. Mater.* **2003**, *13*, 127.

(272) Hochbaum, A. I.; Chen, R. K.; Delgado, R. D.; Liang, W. J.; Garnett, E. C.; Najarian, M.; Majumdar, A.; Yang, P. D. *Nature* **2008**, *451*, 163.

(273) Moore, A. L.; Saha, S. K.; Prasher, R. S.; Shi, L. *Appl. Phys. Lett.* **2008**, *93*, 083112.

(274) Zou, J.; Balandin, A. *J. Appl. Phys.* **2001**, *89*, 2932.

(275) Fardy, M.; Hochbaum, A. I.; Goldberger, J.; Zhang, M. M.; Yang, P. D. *Adv. Mater.* **2007**, *19*, 3047.

(276) Touloukian, Y. S.; Powell, R. W.; Ho, C. Y.; Klemens, P. G. *Thermal Conductivity: Metallic Elements and Alloys*; IFI/Plenum: New York, 1970.

(277) Cahill, D. G.; Pohl, R. O. *Phys. Rev. B* **1987**, *35*, 4067.

(278) Cahill, D. G.; Watson, S. K.; Pohl, R. O. *Phys. Rev. B* **1992**, *46*, 6131.

(279) Boukai, A. I.; Bunimovich, Y.; Tahir-Kheli, J.; Yu, J. K.; Goddard, W. A.; Heath, J. R. *Nature* **2008**, *451*, 168.